Two-Line Atomic Fluorescence for Thermometry in Reactive Flows

Borggren, Jesper

2018

Document Version:
Publisher's PDF, also known as Version of record

Two-Line Atomic Fluorescence for Thermometry in Reactive Flows

Jesper Borggren

LUND
UNIVERSITY

DOCTORAL DISSERTATION

by due persmission of the Faculty of Engineering, Lund University, Sweden.
To be defended in Rydbergsalen, Fysicum, Professorsgatan 1. 09:15 2/2, 2018.

Faculty opponent
Prof. Graham J. Nathan
School of Mechanical Engineering, University of Adelaide, Adelaide

Organization	Document name
LUND UNIVERSITY Department of Physics Box 118 SE–221 00 LUND Sweden	**DOCTORAL DISSERTATION** Date of disputation 2018-02-02 Sponsoring organization
Author(s) Jesper Borggren	

Title

Two-Line Atomic Fluorescence for Thermometry in Reactive Flows

Abstract

Advances in the field of laser-based combustion diagnostics over the past decades have allowed for detailed characterisation, modelling and increased understanding of the complex combustion process. However; many combustion phenomena are still unexplained and there is a continued need for development and application of diagnostic tools to further the understanding of the combustion process. One of the governing physical properties in the combustion process is the temperature due to its exponential effect on the chemical reaction rates. Hence, the work reported throughout this thesis deals with the development and extension of a thermometric technique for reactive flows called two-line atomic fluorescence (TLAF).

In TLAF an atomic species with a suitable electronic structure, that of a three-level lambda-system, is seeded to the flame and the two lower levels are consecutively probed with light. The ratio of the emitted laser-induced fluorescence intensities is governed by the temperature-dependent Boltzmann distribution and used to infer the temperature of the system. TLAF offers several beneficial features such as being independent on the gas composition, strong fluorescence signals and insensitivity to elastic scattering.

The thesis reports on the application of the thermometric technique in a wide range of combustion environments, from low-pressure flat flames, atmospheric jet flames to sooty and particulate laden flames of burning biomass pellets. Two variations of the TLAF technique were performed with external-cavity diode lasers (ECDL): 1) Line shape resolved TLAF where the absorption profile of the two excited levels are recorded as the lasers are tuned and 2) fixed wavelength TLAF where the lasers are stabilized to the peak of the absorption profile.

The accuracy and precision, being figures of merit for any quantitative technique, have been measured and estimated for all the applied cases. An accuracy in the order of 2-3 % at flame temperatures around 1800 K is typical for the TLAF technique and the precision is for many cases below 1 % for averaged measurements. Even with low-power ECDLs imaging and temporally resolved temperature measurements have been demonstrated. A versatile seeding system being able to seed a wide range of burners with an adjustable and constant concentration of the necessary atomic species is also presented.

Key words

Two-line atomic fluorescence, thermometry, laser spectroscopy, diode laser

Classification system and/or index terms (if any)

Supplementary bibliographical information	Language
	English
ISSN and key title 1102-8718	ISBN 978-91-7753-535-5 (print) 978-91-7753-536-2 (pdf)
Recipient's notes	Number of pages: 140 / Price
	Security classification

Two-Line Atomic Fluorescence for Thermometry in Reactive Flows

by Jesper Borggren

LUND
UNIVERSITY

Cover illustration front: Laser-induced fluorescence of indium in a jet flame.

Faculty of Engineering, Department of Physics

Lund Reports on Combustion Physics, LRCP-209
ISBN: 978-91-7753-535-5 (print)
ISBN: 978-91-7753-536-2 (pdf)
ISSN: 1102-8718
ISRN: LUTFD2/TFCP-209-SE

Printed in Sweden by Media-Tryck, Lund University, Lund 2018

Abstract

Advances in the field of laser-based combustion diagnostics over the past decades have allowed for detailed characterisation, modelling and increased understanding of the complex combustion process. However; many combustion phenomena are still unexplained and there is a continued need for development and application of diagnostic tools to further the understanding of the combustion process. One of the governing physical properties in the combustion process is the temperature due to its exponential effect on the chemical reaction rates. Hence, the work reported throughout this thesis deals with the development and extension of a thermometric technique for reactive flows called two-line atomic fluorescence (TLAF).

In TLAF an atomic species with a suitable electronic structure, that of a three-level lambda-system, is seeded to the flame and the two lower levels are consecutively probed with light. The ratio of the emitted laser-induced fluorescence intensities is governed by the temperature-dependent Boltzmann distribution and used to infer the temperature of the system. TLAF offers several beneficial features such as being independent on the gas composition, strong fluorescence signals and insensitivity to elastic scattering.

The thesis reports on the application of the thermometric technique in a wide range of combustion environments, from low-pressure flat flames, atmospheric jet flames to sooty and particulate laden flames of burning biomass pellets. Two variations of the TLAF technique were performed with external-cavity diode lasers (ECDL): 1) Line shape resolved TLAF where the absorption profile of the two excited levels are recorded as the lasers are tuned and 2) fixed wavelength TLAF where the lasers are stabilized to the peak of the absorption profile.

The accuracy and precision, being figures of merit for any quantitative technique, have been measured and estimated for all the applied cases. An accuracy in the order of 2-3 % at flame temperatures around 1800 K is typical for the TLAF technique and the precision is for many cases below 1 % for averaged measurements. Even with low-power ECDLs imaging and temporally resolved temperature measurements have been demonstrated. A versatile seeding system being able to seed a wide range of burners with an adjustable and constant concentration of the necessary atomic species is also presented.

Populärvetenskaplig sammanfattning

Det är numera välkänt att förbränning av fossila bränslen orsakar utsläpp av gaser och partiklar med negativ inverkan på både miljö och människans hälsa. Även om användningen av förnybara energikällor såsom vindkraft och vattenkraft ökar står förbränning av fossila bränslen idag för mer än 80 % av jordens energi- och värmeproduktion. Det är därför av yttersta vikt att förbränningen sker på ett så effektivt och miljövänligt sätt som möjligt för att minska de skadliga utsläppen. För att kunna effektivisera och förbättra användningen av fossila bränslen krävs kunskap och information om de komplexa processer som sker under förbränningen. Denna nödvändiga information erhålls oftast genom experimentella mätningar. Utvecklandet av optiskt baserade mätmetoder har de senaste årtionden avsevärt ökat kunskapen och förståelsen för förbränningsprocesser. Dessa mätmetoder, speciellt baserade på lasrar, har flera fördelaktiga egenskaper, som gör dem till det optimala diagnostiska verktyget. Optiska mätningar är beröringsfria, det vill säga de påverkar inte mätobjektet under mätningen så som till exempel en fysisk mätspets hade ändrat flödet i flamman. Mätningar kan t.ex. även göras ämnesspecifika, ögonblickliga och både ge två- och tredimensionell mätdata.

Under förbränningsförloppet interagerar flertalet fysikaliska och kemiska storheter och processer. En av de grundläggande fysikaliska storheterna som styr förbränningsprocessen är temperaturen på grund av dess exponentiella påverkan på de kemiska reaktionernas hastighet. Det krävs därför detaljerad information om temperaturen för att i många fall uppnå en fullständig förståelse för förbränningsprocessen. Precisa och exakta temperaturmätningar är därför hett eftertraktade. I den här avhandlingen presenteras utvecklingen av en laserbaserad teknik, kallad atomär två-linje fluorescens, för temperaturmätningar i förbränningsmiljöer.

Principen bakom tekniken bygger på att atomer som, genom att interagera med laserljus, får ett högre energitillstånd (exciteras) för att efter en kort stund (nanosekund) skicka ut ljus i alla riktningar i rummet, så kallad fluorescens. Fluorescensens ljusstyrka mäts i mitt arbete i två dimensioner med en kamera. Genom att endast undersöka fluorescensen från atomer med väldigt specifika egenskaper kan temperaturen i den gas atomerna befinner sig i härledas från den uppmätta ljusstyrkan. Tekniken har flera fördelar gentemot andra laserbaserade mätmetoder. En stor fördel är att tekniken är oberoende av vilken typ av molekyler som gasen innehåller, vilket är en stor fördel eftersom det ofta är svårt att veta den exakta gassammansättningen i förbränningsmiljöer. Mätningar kan med fördel också utföras i flammor med mycket sot eller partiklar och den starka fluorescensen från atomerna gör det möjligt att använda små kompakta diodlasrar som ljuskällor. Nackdelen med tekniken är att atomerna som används i tekniken inte existerar naturligt i förbränningsmiljöer och måste introduceras på konstgjord väg. Detta problem har lösts genom att ett system för att

tillförlitligt förse olika typer av förbränningsmiljöer med det atomära ämnet har utvecklats. Systemet beskrivs i en av de i avhandlingen inkluderade artiklarna.

Resterande artiklar i avhandlingen handlar om utvecklingen av atomär två-linje-fluorescens för temperaturmätningar samt dess applikationer. Temperaturmätningar har utförts i bland annat lågtrycks och atmosfäriska flammor och två olika atomära grundämnen har jämförts för att undersöka vilken som passar bäst i olika mätsituationer. Temperaturmätningar under förbränningen av träpellets, en miljö som är extremt krävande för optiskdiagnostik på grund av den sotiga flamman, avhandlas också i en artikel.

List of publications

This thesis is based on the following publications, referred to by their Roman numerals:

I R. Whiddon, B. Zhou, **J. Borggren**, M. Aldén and Z.S. Li
Vapor phase tri-methyl-indium seeding system suitable for high temperature spectroscopy and thermometry, Review of Scientific Instruments, 86, 093107 (2015)

II **J. Borggren**, I. Burns, A.L. Sahlberg, M. Aldén and Z.S. Li
Temperature imaging in low-pressure flames using diode laser two-line atomic fluorescence employing a novel indium seeding technique, Applied Physics B, 122:58 (2016)

III **J. Borggren**, W. Weng, A. Hosseinnia, P.E. Bengtsson, M. Aldén and Z.S. Li
Diode laser-based thermometry using two-line atomic fluorescence of indium and gallium, Applied Physics B, 123:278 (2017)

IV **J. Borggren**, W. Weng, M. Aldén and Z.S. Li
Temperature measurements above a burning wood pellet using diode-laser based two-line atomic fluorescence., Applied Spectroscopy, Published Online

V W. Weng, **J. Borggren**, B. Li, M. Aldén and Z.S. Li
A novel multi-jet burner for laminar flat flames of wide range of temperatures and oxygen concentrations: Valuable for quantitative optical diagnostics in biomass gasification/combustion, Review of Scientific Instruments 88, 045104 (2017)

Publications not included in this thesis:

Z. Li, **J. Borggren**, and E. Kristensson
Single-shot multi-species visualizations using FRAME, Under Review Combustion and Flame

M. Jonsson, **J. Borggren**, M. Aldén and J. Bood
Time-resolved spectroscopic study of photofragment fluorescence in methane/air mixtures and its diagnostic implications, Applied Physics B, 120:4, 587-599 (2015)

K. Larsson, M. Jonsson, **J. Borggren**, E. Kristensson, A. Ehn, M. Aldén, and J. Bood
Single-shot photofragment imaging by structured illumination,, Optics Letters 40, 21, 5019-5022 (2015)

M. Jonsson, K.Larsson, **J. Borggren**, M. Aldén, and J. Bood
Investigation of ps-PFLIF for detection of hydrogen peroxides in laminar flames, Combustion and Flame, (2016)

S. Reifarth, E. Kristensson, **J. Borggren**, A. Sakowitz and H.E. Angstrom
Analysis of EGR/Air Mixing by 1-D Simulation, 3-D Simulation and Experiments, SAE Technical Paper 2014-01-2647 (2014)

Dedicated to you, the reader
And Hugo for letting me finish this, almost, in peace.

Innehåll

Chapter 1

Introduction

Pollution from combustion is one of the major global challenges in this day and age due to the, well known, adverse effects on the climate and human health. Combustion of fossil fuels is currently producing more than 80% of the energy needs of the world and while progress is made towards replacing fossil fuels with cleaner renewable sources they will continue to play a major role in the decades to come. It is thus of utmost importance to improve the combustion process by increasing the efficiency and reducing pollutant emissions both to adhere to new laws and regulations as well as it being economically sound. Improvement requires detailed knowledge of the combustion process to allow for a move from an ad hoc design perspective of combustion devices to a more structured design plan.

Combustion can briefly be described as the process of oxidation of a fuel to release chemically bound energy, most often in the form of heat. This can either be used for heating purposes or for generation of electrical energy often by means of driving a generator connected to a turbine. Combustion is, however, a complex phenomenon involving chemical reactions between hundreds of molecular species interacting in turbulent flows at temporal and spatial scales spanning many orders of magnitude. The complex interaction of many physical and chemical properties requires simultaneous in-situ measurements to decouple the measured quantities. Due to the high demands on the experiments and equipment it is not until the technical advancements of the last few decades that really has allowed for the possibility to extensively investigate the physical and chemical processes of combustion.

In recent times great strides have been taken to model the combustion process using both computational fluid dynamics (CFD) and detailed chemical kinetic models. These methods have become a widely established tools for design of combustion devices. To further

increase the understanding of the combustion process and to aid in the improvement and development of better models experimental measurements of high quality are essential.

Experimental techniques can crudely be divided into two categories, intrusive and non-intrusive measurements. Intrusive techniques often involve inserting some type of probe in the measurement region, e.g., a thermocouple for temperature measurements or a sample probe for a mass spectrometer. For certain applications intrusive techniques may provide valuable information even though perturbations are introduced in the measurement. However, non-intrusive techniques have the advantage of not perturbing the combustion environment and possibly distort the result and should therefore be preferred over the intrusive equivalent. Non-intrusive techniques are often based on optical principles by probing molecules and atoms with light while recording the physical response to provide information of properties such as temperature, species concentrations and flow fields [1, 2]. A powerful tool for optical diagnostics in combustion was found with the advent of lasers – allowing for measurements that would otherwise be unattainable. Lasers offers many beneficial features, e.g., high brilliance to improve the signal strength, short laser pulses for instantaneous measurements, imaging and volumetric capabilities, species specificity and image sequences with a high temporal resolution.

Of the many physical properties interacting during the complex combustion process temperature is one of the most important. Temperature governs the combustion process due to its strong dependence on the chemical reaction rates. Information of the local temperature is always highly demanded due to the strong influence on the combustion process and there are a multitude of laser-based techniques available for temperature measurements [3, 4].

This thesis reports on the development of laser-based combustion diagnostics and especially that of a thermometric technique called two-line atomic fluorescence (TLAF). TLAF is a technique that can provide instantaneous two-dimensional temperature information in a large variety of combustion environments, from low-pressure chambers, atmospheric flames to high-pressure applications such as in internal combustion engines with the needed accuracy and precision.

In Chapter 2 the theory of two-line atomic fluorescence is discussed. The derivation of temperature from the induced fluorescence signals is presented and possible error sources are reviewed. Chapter 3 deals with the most essential experimental equipment that was used for the development of the TLAF technique such as the light sources and seeding system. Experimental results related to the included papers are discussed in Chapter 4 and in the last Chapter 5 the thesis work is summarized and an outlook of future work is presented.

Chapter 2

Theory

The work presented in this thesis has mainly focused on the development of a thermometric technique, called two-line atomic fluorescence (TLAF), for temperature measurements in, especially, hot reactive flows of combustion devices, e.g. in the flame of a burner. Hence, it may be natural to ask: what is temperature and what is the physical definition of this quantity? This is what the first sections of this chapter deals with. In subsequent sections the theory of TLAF is explained and two variations of TLAF used for temperature measurements in the included papers are presented.

2.1 What is Temperature?

The following section is based on references [5–8]. The concept of temperature is widely known, i.e. is something hot or cold? But if one were to scientifically investigate the effect of temperature on a system, be it an object or gas, e.g., a flame, it would most probably not suffice to answer that the flame is really hot. The temperature needs to be quantified in relation to a universally defined temperature scale. However, before defining a temperature scale it is useful to understand how objects with a temperature behave. For this end the zeroth law of thermodynamics can be used which is commonly used to define the concept of temperature, stating that

> **Two systems, each separately in thermal equilibrium with a third, are in equilibrium with each other.**

Thermal equilibrium is a steady-state reached when there is no net transfer of energy (heat) between two bodies in thermal contact. Assume there are two bodies with differing temperatures T_1 and T_2. If $T_1 > T_2$ and the two bodies are in thermal contact, heat will flow from the first body to the second. After a sufficient time has passed the two bodies will reach thermal equilibrium and will thus be said to be of the same temperature. A thermometric measurement utilizes the response of a temperature sensitive and observable property such as a volume expansion of a liquid or a change in electrical resistance to measure the temperature. When the thermometric medium is in thermal equilibrium with the object to be measured the temperature is read from a calibrated scale. This scale should be independent of the thermometric medium. The Kelvin scale is an absolute and invariable temperature scale that measures the thermodynamic temperature. The absolute scale is defined by zero being the lowest physically attainable temperature of a system and a second clearly defined temperature point, necessary to fully establish a linear temperature scale, is the triple point of water at 273.16 K. The triple point is the temperature and pressure when the three phases of water are in equilibrium.

To understand what happens inside a body when the temperature changes, the behaviour of the atoms and molecules in the body has to be taken into consideration and due to the extremely large number of molecules in a system a statistical approach is necessary. In statistical thermodynamics temperature is defined as *"the parameter that show the most probable distribution of populations of molecules over the available states for a system at thermal equilibrium"* [6]. The distribution of a population can also be called distribution of macrostates where the macrostates comprises of many microstates. A microstate contains detailed information of every particle in a system and each particle is distinguishable from another while in the macrostate particles are not distinguishable and describes the ensemble of states for all particles. In a gas the microstate may be the description of the position and energy of every molecule and the macrostate can be the thermodynamic properties such as pressure and temperature. The Boltzmann distribution relates the energy of the system to the probability of finding a system in a certain energy state E_i as

$$P_i = \frac{g_i \cdot e^{-E_i/k_B T}}{\sum_i g_i \cdot e^{-E_i/k_b T}} \tag{2.1}$$

where P_i is the probability to find a system in state i, k_B the Boltzmann constant and T the temperature. The macroscopic properties can be related to the probability of finding the system in a certain microstate through the Boltzmann distribution, e.g. the Boltzmann distribution can be used to find the relationship between the temperature of a gas and the velocity of the molecules such that the mean kinetic energy is $W_{kin} = \frac{3}{2} k_b T$ for mono-

atomic gases. This means that at absolute zero temperature the thermal motion of molecules ceases.

2.1.1 The Role of Temperature in Combustion

Temperature is one of the governing physical properties in a combustion process due to the strong exponential temperature dependence on the chemical reaction rate. The rate coefficient k, deciding the speed at which a reaction occur, is at combustion temperatures often expressed with a modified Arrhenius equation given by

$$k = AT^n e^{-E/RT} \tag{2.2}$$

A is the pre-exponential, E the activation energy and R is the gas constant. Due to the exponential nature a small change in temperature ΔT often results in a large change of the rate coefficient and precise and accurate temperature measurements are thus highly demanded to understand the combustion process. Temperature information is also required in other laser-based combustion diagnostics such as in concentration measurements.

In the typical combustion processes of hydrocarbons the temperatures range from 300 K in the unburned region to more than 2000 K in the product zone. The thermometric medium should in the optimal case be sensitive over the complete temperature range. A thermometric medium naturally present in the combustion region are the molecules themselves which can be exploited in laser-based diagnostics. Some of the physical temperature-dependent properties are, e.g., the translational movement of the molecules, the gas density, and the population of electronic, vibrational and rotational levels. Simultaneously measurements of these different temperature-sensitive properties may sometimes yield widely differing temperatures. In this case the probe volume is not in thermal equilibrium and *"the flame temperature cannot basically be defined in an unambiguous way"* [9]. A multitude of optical techniques have been developed to probe the temperature-dependent properties of these molecules with light and a brief review of these techniques is given in the following section.

2.2 Laser-Based Thermometric Techniques

Rayleigh scattering is a thermometric technique in which the temperature is deduced from the number density-dependence of the scattered signal [10]. The technique has certain limitations due to the low molecular scattering cross-section and sensitivity to elastic scattering

from particles and surfaces, although, it is possible to spectrally filter the strong elastic scattering to perform measurements in scattering flows [11, 12]. Additional complexities come from the scattering signal being dependent on the gas composition which in combustion environments, and especially in turbulent flames, often are unknown.

Coherent anti-Stokes Raman spectroscopy (CARS) is a mature thermometric technique and often seen as a gold standard in laser-based thermometry thanks to the good accuracy and precision [3]. In CARS, a non-linear interaction of electromagnetic waves probes the temperature-dependent vibrational and rotational population of molecules. The generated signal is a coherent laser beam that follows the direction of the phase-matching condition resulting in a strong signal. Recent advances has extended CARS from point measurements to both one and two dimensions [13, 14] and both femto- and picosecond lasers have been adapted to provide single-shot and high repetition rate measurements [15].

There are a plenitude of thermometric techniques based on the laser-induced fluorescence of atoms and molecules, e.g., NO, OH, and several aromatic hydrocarbons [16]. In NO- and OH-based thermometry the population distribution is probed by a tunable laser and the temperature is deduced from a time-demanding excitation scan [17–19]. Alternatively two temperature sensitive lines are probed sequentially and the fluorescence ratio is used to infer the temperature of the system [20]. This later approach allows for instantaneous temperature measurements.

Other notable thermometric techniques include thermographic phosphor tracer particles [16] and laser-induced grating spectroscopy [2, 21]. Although there is an abundance of thermometric techniques available for gas phase measurements the high demand of temperature information drives the development of more accurate, applicable and robust measurements techniques. The rest of this thesis details the development and extension of two-line atomic fluorescence – a thermometric technique based on atomic fluorescence.

2.3 Two-Line Atomic Fluorescence

Two-line atomic fluorescence is a ratiometric thermometric technique in which two lower lying electronic levels of an atom are sequentially excited to a common upper state and a ratio is formed from the two subsequently detected fluorescence signals. The detected fluorescence signal is proportional to the population of the excited ground level which is governed by the temperature-dependent Boltzmann distribution. This allows for the temperature to be derived from the ratio of the fluorescence signals.

TLAF offers many beneficial features to the previously reviewed thermometric techniques. The ratiometric approach makes the technique independent of gas composition which is a

great advantage in combustion environments where the gas composition is often unknown. The atomic fluorescence is also advantageous to molecular fluorescence in regards to both signal strength and simplicity of the electronic configuration. Atomic transitions have a much higher transition cross-section than molecules and are free from vibrational and rotational modes. In TLAF the detection of the fluorescence may also be wavelength shifted so that elastically scattered interferences can be spectrally filtered. TLAF does, however, require the introduction of an atomic species, with suitable electronic configuration, not normally present in the combustion environment. Atoms with suitable electronic structures are found in the Group III metals in the periodic table such as gallium, indium, thallium and lead. Compared to thermometric techniques probing naturally present molecules such as OH or CH the seeded atomic species is not as limited to certain regions in the flames and the concentration of the seeded species can be adjusted to increase signal levels. The excitation wavelengths are, for the relevant atomic elements, in the visible region as compared to OH and NO where excitation wavelengths are conducted in the UV-region. The use of visible light reduces absorption and interferences from polycyclic aromatic hydrocarbons (PAH) that are abundant in rich flames.

2.3.1 Three-Level Lambda System

The electronic configuration of the relevant levels for TLAF of the Group III metals are shown in Figure 2.1. The ground state is split into two sublevels, $P_{1/2}$ and $P_{3/2}$, due to the spin-orbit coupling. These two sublevels are each further split into several hyperfine levels. The $P_{1/2}$ has two hyperfine levels and $P_{3/2}$ has four hyperfine levels. The upper state $S_{1/2}$ has two hyperfine levels resulting in the transition $P_{1/2} \rightarrow S_{1/2}$ having four allowed hyperfine transitions and $P_{3/2} \rightarrow S_{1/2}$ having six allowed hyperfine transitions. The relative intensities of the hyperfine transitions is calculated from the Clebsch-Gordan coefficients [22]. The energy splitting ΔE between the two lower levels, $P_{1/2}$ and $P_{3/2}$, is a crucial parameter for the accuracy and precision in TLAF as will be shown later.

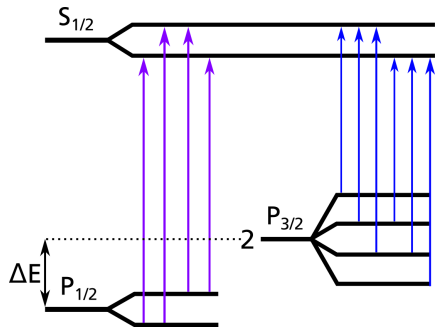

Figure 2.1: The electronic configuration of a three level lambda system commonly used in TLAF. The ground state is split into two fine structure levels $P_{1/2}$ and $P_{3/2}$ and these are further split into two and four hyperfine levels respectively. The allowed hyperfine transitions are marked with arrows.

2.3.2 Detection Schemes

There are two different detection schemes possible in TLAF, schematically shown in Figure 2.2. In detection scheme 2.2a the non-resonant fluorescence is detected upon subsequent excitation of the two lower levels. This usually requires two detectors or as shown in Paper V the use of a stereoscope mounted with two filters. Using this scheme elastically scattered light can be spectrally filtered which is very useful in particle-laden and sooting flames. However, the detection system needs to normally be calibrated due to differences in both the signal collection as well as the quantum yield at the two different wavelengths. The calibration is usually performed with a second thermometric measurement to calculate a calibration factor. Due to the need for a calibration measurement, usually conducted with a thermocouple, it could be argued that the temperature measurement using this detection scheme can not be better than the accuracy of the calibration technique.

In detection scheme 2.2b only fluorescence of one wavelength is acquired, one non-resonant (F_a) and one resonant (F_b) fluorescence signal. The need for two detectors is avoided and thereby also the need for a calibration, resulting in a calibration-free TLAF technique. The experimental setup is also simplified and in situations with limited optical access the requirement of only a single detector is useful, such as reported on in Paper II. The drawback of this scheme is that explicit knowledge of the Einstein coefficients is necessary, see Equation 2.11, which introduces a systematic error in the temperature measurements. Detection to the upper level $P_{3/2}$ is often preferred due to mainly three reasons: *i*) A higher transition probability by a factor of approximately two, *ii*) lower fluorescence trapping due to a lower population in the upper level and *iii)* less interference from chemiluminescence of natur-

ally occurring species such as CH and C_2. This detection scheme is, however, sensitive to elastic scattering.

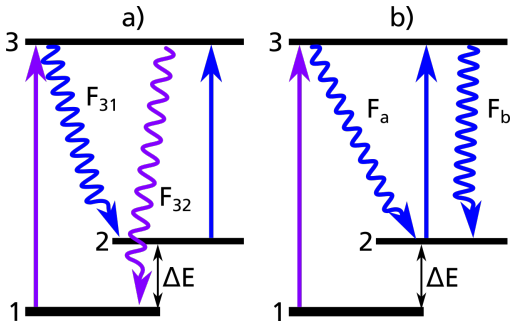

Figure 2.2: Two possible detections schemes in TLAF. In detection scheme *a* the non-resonant fluorescence is detected. In *b* only fluorescence to one level is detected independent on the laser excitation wavelength.

2.3.3 Temperature Derivation

In TLAF the temperature is, as previously mentioned, derived from the ratio of the two fluorescence signals detected upon subsequent excitation of the two lower ground states. The detected fluorescence F from excitation of level i is proportional to the population of excited state N_3 as:

$$F = \Delta E_{3i} N_3 A_{3i} \Omega \tag{2.3}$$

where ΔE_{3i} is the energy of the emitted photon, A_{3i} is the Einstein coefficient for the corresponding transition and Ω contains geometric information of the detection and illumination, e.g, collection angle and laser beam area. The subscripts are consistent with Figure 2.1. The fluorescence signal is proportional to the number density of the excited state N_3 and this population can in turn be related to the population of the excited ground level N_i through rate equations taking all excitation and de-excitation processes into consideration. The transition rates R_{ij} between levels i and j are for a general three-level system presented in Figure 2.3 and the corresponding rate equations are shown in Equation 2.4. The transition rates R_{ij} for excitation of the Stokes and anti-Stokes transtions are defined in Table 2.1 (from Manteghi et al. [23]).

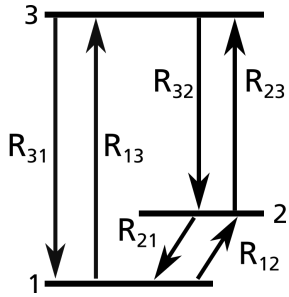

Figure 2.3: The transitions in a three level system. The R-terms are defined in table Table 2.1.

$$\begin{aligned}\frac{dn_1}{dt} &= -(R_{13}+R_{12})n_1 + R_{31}n_3 + R_{21}n_2 \\ \frac{dn_2}{dt} &= -(R_{23}+R_{21})n_2 + R_{32}n_3 + R_{12}n_1 \\ \frac{dn_3}{dt} &= -(R_{31}+R_{32})n_3 + R_{13}n_1 + R_{23}n_2\end{aligned} \tag{2.4}$$

Table 2.1: Transition rates R. A and B are the Einstein coefficients for spontaneous emission, stimulated emission and stimulated absorption. Q is the quenching, I^{ν} is the irradiance of the laser and c the speed of light.

Excitation $1 \rightarrow 3$ (Stokes)	Excitation $2 \rightarrow 3$ (anti-Stokes)
$R_{13} = B_{13}I^{\nu}_{13}/c$	$R_{13} = 0$
$R_{31} = B_{31}I^{\nu}_{13}/c + Q_{31} + A_{31}$	$R_{31} = Q_{31} + A_{31}$
$R_{23} = 0$	$R_{23} = B_{23}I^{\nu}_{23}/c$
$R_{32} = Q_{32} + A_{32}$	$R_{32} = B_{32}I^{\nu}_{32}/c + Q_{32} + A_{32}$

The transitions between level 1 and 2 (R_{12} and R_{21}) can be assumed to be induced solely by collisions and can thus be related through detailed balancing [23] with the degeneracies of each level g and energy gap ΔE_{21}.

$$\frac{R_{12}}{R_{21}} = \frac{g_2}{g_1}\exp\left(-\frac{\Delta E_{21}}{k_B T}\right) \tag{2.5}$$

The population of the excited state, i.e. the fluorescence signal, follows a non-linear behaviour as a function of laser power. At low laser powers the fluorescence is said to be in the linear regime as the fluorescence signal is linearly proportional to the incident laser power. When the laser power is increased the fluorescence signal is no longer linear to the incident laser power instead it moves asymptotically towards a maximum fluorescence intensity defined by the Einstein A and B coefficients. The saturation regime is reached when the fluorescence signal does not increase with increasing laser power. Between the linear and saturation regime is the so called non-linear regime. It is possible to derive a general analytical temperature expression from the given transition rates that is valid for all regimes [24]; however, this expression is very convoluted and requires detailed knowledge of the transition rates. The temperature expression may instead be simplified with certain assumptions

for the different regimes. The temperature expression of TLAF is thus dependent on the excitation regime.

In the linear regime the fractional populations of all states are assumed to be unaffected upon laser excitation and remain in thermal equilibrium. The populations of levels 1 and 2 are not affected by the relaxation R_{12} and R_{21} as they are already in thermal equilibrium and the relaxation can be neglected in the linear regime. The stimulated emission can also be neglected due to the non-existent population in the excited state at thermal equilibrium. The population of the upper state upon excitation from level i is for the linear regime simplified to:

$$N_3 = \frac{N_i I_{i3}^{\nu} B_{i3}}{c \cdot (A_{31} + A_{32} + Q_{31} + Q_{32})} \tag{2.6}$$

Combining Equation 2.3 and 2.6 an expression for the fluorescence ratio can be derived. This fluorescence ratio is different for the two detection schemes due to the fluorescence signal being proportional to the detected wavelength. For the resonant detection scheme the ratio becomes:

$$\frac{F_a}{F_b} = \frac{N_1 I_{13}^{\nu} B_{13}}{N_2 I_{23}^{\nu} B_{23}} \tag{2.7}$$

In thermal equilibrium the populations of the two probed levels 1 and 2 are related through the Boltzmann distribution.

$$\frac{N_1}{N_2} = \frac{g_1}{g_2} \exp\left(-\frac{\Delta E}{k_B T}\right) \tag{2.8}$$

From Hilborn [25] the Einstein A coefficient for spontaneous emission can be related to the Einstein B coefficient for stimulated absorption as:

$$A_{3i} = B_{i3} \frac{g_3}{g_i} \frac{8\pi h}{\lambda_{i3}^3} \tag{2.9}$$

The laser irradiance depends on both the normalized laser overlap $L(\nu)$ and the normalized absorption profile $g(\nu)$ as a function of frequency ν.

$$I^{\nu} = I^0 \int_{\nu} L(\nu) g(\nu) d\nu \tag{2.10}$$

I^0 is the incident laser irradiance and the intregal is known as the line overlap integral [3]. Combining Equation 2.7,2.8, 2.9 and 2.10 the temperature expression as a function of the fluorescence ratio for the resonant detection scheme becomes [26]:

$$T = \frac{\Delta E/k_B}{\ln\left(\frac{F_a}{F_b}\right) + \ln\left(\frac{I_{23}^0 \int_\nu L_{23}(\nu) g_{23}(\nu) d\nu}{I_{13}^0 \int_\nu L_{13}(\nu) g_{13}(\nu) d\nu}\right) + 3\ln\left(\frac{\lambda_{23}}{\lambda_{13}}\right) + \ln\left(\frac{A_{23}}{A_{13}}\right)} \tag{2.11}$$

For the non-resonant detection scheme presented in Figure 2.2a the fluorescence ratio in the linear regime is given by:

$$\frac{F_{31}}{F_{32}} = \frac{\lambda_{13}}{\lambda_{23}} \frac{N_1 I_{13}^\nu B_{13} A_{32}}{N_2 I_{23}^\nu B_{23} A_{31}} \frac{\Omega_1}{\Omega_2} \tag{2.12}$$

and the temperature as a function of this fluorescence ratio becomes

$$T = \frac{\Delta E/k_B}{\ln\left(\frac{F_a/I_{13}^0}{F_b/I_{23}^0}\right) + 4\ln\left(\frac{\lambda_{23}}{\lambda_{13}}\right) + C_t} \tag{2.13}$$

where C_t is a constant accounting for differences in collection efficiencies, quantum efficiencies of the detectors at the two wavelengths and also in this case the line overlap integral [27, 28]. C_t is normally calibrated from a second thermometric technique, most often using a thermocouple; however, it could in principle be quantified without a calibration. Comparing the temperature expressions for the two detection schemes, Equation 2.13 and 2.11, it is observed that the resonant detection scheme requires explicit knowledge of the Einstein A coefficients but may avoid the need for a calibration measurement if the overlap between the lasers and absorption profiles are known.

The signal-to-noise ratio of the detected fluorescence signal is increased in the non-linear and saturation excitation regime. These excitation regimes are not used in the included papers in this thesis and the reader is directed to the referenced papers for the explicit temperature expressions in these regimes. In non-linear TLAF, developed by Medwell et al. [29, 30], the temperature expression involves two more calibration constants acquired from the fluorescence power-dependence curves of the two excited transitions. For TLAF in the saturated regime the temperature expression comes from the detailed balancing of the relaxation between level 1 and 2 and not the fractional population at thermal equilibrium [23].

2.3.4 Line Shape Fitting

In the development of TLAF reported throughout this thesis external cavity diode lasers (ECDLs) have been the light source employed for excitation. ECDLs provide continuously tunable and narrow line-width light allowing for the characterization of the absorption profile, also known as the line shape, and thereby calculation of the overlap function. Accurate simulations and fitting of experimentally measured line shapes of the probed atomic species are crucial for evaluation of the temperatures in TLAF when narrow-band lasers are used, as discussed in the next Section 2.3.5. Below follows a description of the fitting process.

An experimental line shape is acquired by tuning a laser across the absorption profile and recording the fluorescence signal. As shown in Figure 2.1, the line shape of one transition for the group III metals used in TLAF is a combination of either four or six hyperfine level transitions. Each hyperfine transition is broadened due to mechanisms related to mainly two physical quantities, temperature and pressure. A brief explanation of the broadening effects are given here, for a more rigorous explanation see e.g., [3, 31, 32]. The temperature broadening is caused by the Doppler effect, i.e. the moving atoms will shift the frequency of the emitted light depending on if they are moving towards or away from a stationary detector. The velocity distribution of the moving atoms follows a Gaussian distribution and thus gives rise to a Gaussian shaped broadening. The pressure broadening is caused by perturbations of the levels of the excited atoms due to adjacent molecules and collisions. The broadening effect is dependent on the gas composition, pressure and number density. The line shape arising from the pressure broadening is a Lorentzian distribution. The total broadening effect due to the temperature and pressure is a convolution of the Lorentzian and Gaussian broadening, the so called Voigt profile [3]. In atmospheric flames the Lorentzian and Gaussian broadening component is in the same order of magnitude for the elements of interest in TLAF.

In the work presented in this thesis the whole line shape was simulated by the summation of a Voigt profile for each hyperfine transition of the probed level. The relative intensity of each hyperfine transition was determined by the Clebsch-Gordan coefficients [22] and the relative frequency spacing between the hyperfine levels was taken from litterature. Relevant data for the atomic species used in this thesis can be found in Chapter 5.1. The Voigt profiles themselves were generated by the convolution of a Gaussian distribution, determined by the temperature and mass of the species, and a Lorentzian distribution accounting for the pressure broadening. The Lorentzian distribution is, as mentioned, a function of temperature, pressure and gas composition. As the local gas composition or collisional cross-sections (or both) often are unknown it is difficult to make a physical model describing the actual Lorentzian contribution to the Voigt profile [33]. The pressure-broadening

can be simplified with the use of a reference collisional broadening parameter $\Delta\nu_{ref}$ as explained by Burns et al. [34]. The reference pressure broadening parameter is measured in a flame with a known temperature, pressure and gas composition by fitting a line shape to the experimental data and adjusting only the reference collisional broadening. The pressure broadening in an unknown flame $\Delta\nu_L$ can then be calculated from Equation 2.14 assuming the gas composition is somewhat similar as for the reference measurement.

$$\Delta\nu_L = \Delta\nu_{ref} \cdot \left(\frac{T_{ref}}{T}\right)^{0.7} \cdot \frac{P}{P_{ref}} \tag{2.14}$$

T_{ref} and P_{ref} are the temperature and pressure at which the reference measurement was conducted. The exponential, in this case 0.7, describes the temperature dependence of the Lorentzian broadening and is derived from the impact broadening theory explained more in detail in [28, 34–36].

The pressure broadening was measured in methane/air flames by Burns et al. [34] and it was argued that for hydrocarbon flames with air as oxidizer the reference broadening is mainly determined by collisions with nitrogen and due to the abundance of nitrogen the pressure broadening was assumed to be rather constant for different fuels or equivalence ratios.

Knowledge of the temperature and pressure dependence of the Lorentzian and Gaussian broadenings allows for line shape simulations and fitting of the experimental line shapes. A least-squares curve fitting algorithm included in the MatLab software was utilised to fit the experimental data with a simulated line shape for all the work presented throughout this thesis. The number of fitted parameters was dependent on the application and the possible parameters were: amplitude, background, temperature and reference pressure broadening.

The line shapes of the two selected transitions of indium are shown in Figure 2.4. These line shapes were recorded in a flat flame with equivalence ratio 1.2 on a Perkin-Elmer porous plug burner seeded with $InCl_3$ dissolved in water. More information about the burner is found in [37]. A simulated line shape fitted to the data is presented together with the experimental data points. The simulation of the line shape is essential for the temperature evaluation when lasers with line widths much smaller than the absorption profile are utilised due to the required knowledge of the spectral overlap between the laser and absorption profile. The advantage is that knowledge of the overlap function removes the need for a second thermometric technique to calibrate the TLAF measurements as shown in Equation 2.11. The TLAF measurements could thus be argued to be calibration-free.

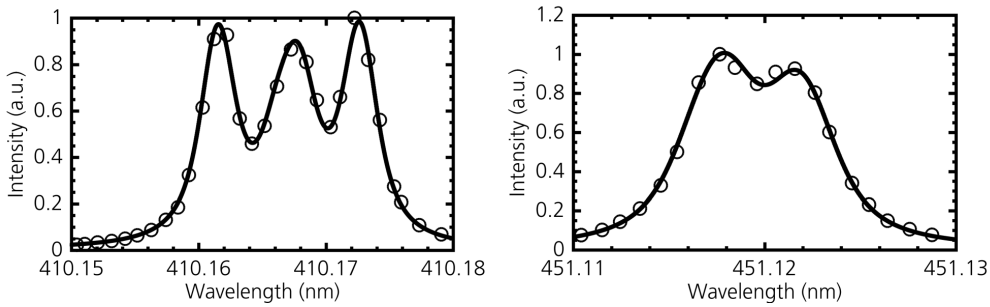

Figure 2.4: The experimental line shape (circles) of the two transtions of indium recorded in a flat flame at ambient pressure with equivalence ratio 1.2 seeded with water dissolved $InCl_3$. The curves show the best fitted line shapes. The wavelength scale was measured with a wavemeter (WS-6, HighFinesse). *Left* - $5P_{1/2} \rightarrow 6S_{1/2}$ transition and *Right* - $5P_{3/2} \rightarrow 6S_{1/2}$ transition of indium.

The dependence of temperature on the line shape makes it possible to deduce the temperature from the line shape of a single transition. This technique, termed one-line atomic fluorescence (OLAF), has been demonstrated by Burns et al. [34] in atmospheric flames. In OLAF the temperature is derived from the fitting of the experimental line shape and the fitting algorithm is thus of great importance to achieve correct temperatures. Even though no OLAF was used in the work presented in the included papers the fitting algorithm is still important in TLAF when narrow-line width lasers are used.

2.3.5 Temperature Evaluation

There are two possible excitation methods in TLAF when ECDLs are used: The lasers can either be at a fixed wavelength in relation to the absorption profile (in this thesis referred to as fixed wavelength TLAF) or the lasers can be tuned across the absorption profiles while the LIF signals are recorded (referred to as line shape resolved TLAF). In measurements where the lasers are tuned, the time resolution is limited by either the frequency of the laser scanning or by the response of the detector, e.g. for point measurements the laser scanning frequency is the limiting factor while in imaging applications it is most often the detector that limits the time resolution, requiring the use of a fast camera. Fixed wavelength TLAF can have a much better temporal resolution, limited mostly by how fast it is possible to switch between the lasers and the acquisition speed of the camera. The two methods differ regarding the temperature evaluation procedure and will be discussed in the following section.

2.3.6 Line Shape Resolved TLAF

In Paper II a line shape resolved TLAF measurements were conducted in which the line shapes of the two transitions of indium were acquired for different positions in a low-pressure flame. Experimental line shapes of the two transitions of indium are shown in Figure 2.5 recorded at a pressure of 50 mbar in a flame with equivalence ratio 1.42. Compared to the line shapes recorded at atmospheric pressures, shown in Figure 2.4, the individual hyperfine transitions are seen to be more pronounced due to the substantially lower pressure.

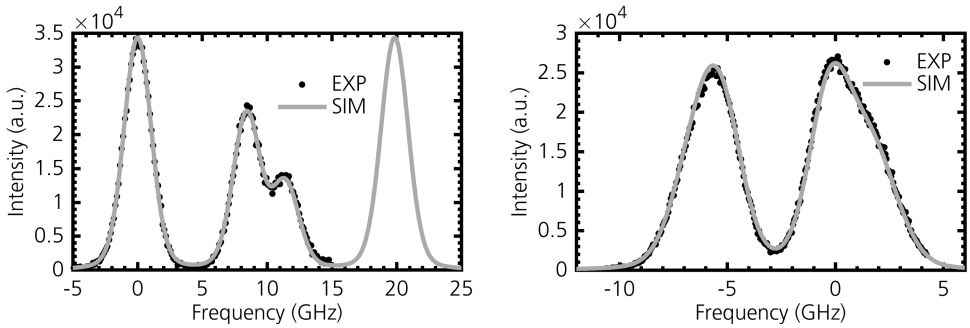

Figure 2.5: Line shape of the two transtions of indium recorded in a low pressure flame at a pressure of 50 mbar and equivalence ratio ϕ = 1.42. *Left* - $5P_{1/2} \rightarrow 6S_{1/2}$ transition and *Right* - $5P_{3/2} \rightarrow 6S_{1/2}$ transition of indium.

The TLAF expression to derive the temperature with the entire line shape can be written somewhat differently to the temperature expression derived in Equation 2.11. When the lasers are tuned over the absorption profile the fluorescence intensity have to be integrated with respect to the laser wavelength (frequency) over the entire line shape. The temperature expression for the resonant detection scheme (see Section 2.3.2) is thus given by Equation 2.15.

$$T = \frac{\Delta E/k}{ln\left(\frac{\int_0^\infty \frac{F_a(\nu)}{I_{13}(\nu)}d\nu}{\int_0^\infty \frac{F_b(\nu)}{I_{23}(\nu)}d\nu}\right) + 3ln\left(\frac{\lambda_{32}}{\lambda_{31}}\right) + ln\left(\frac{A_{32}}{A_{31}}\right)} \tag{2.15}$$

The fluorescence signal is integrated over the whole line shape to evaluate the temperature and in the optimal case the entire line shape would be recorded to allow the experimentally measured signal to be integrated. However, due to the limited scanning range of most ECDLs it is not possible to scan the entire line shape. Instead, a simulated line shape is fitted to the experimental data to generate integrable line shapes allowing for the temperature to

be evaluated. In data with low signal-to-noise ratios the fitting procedure also makes it possible to evaluate a temperature that would otherwise be difficult.

2.3.7 Fixed Wavelength TLAF

For TLAF measurements with fixed wavelength lasers there are two cases to consider: the use of narrow line-width lasers (laser line width < absorption profile), in which case the overlap between the laser and absorption profile has to be explicitly known, or the use of wider line-width lasers (laser line width in the same order or greater than the absorption profile) where the spectral overlap is usually calibrated with a second thermometric technique, see Equation 2.13. The width of the absorption profile of indium is, as seen in Figure 2.4 for flame temperatures, in the order of 30 GHz. Most commercial dye laser systems, frequently used for TLAF, have specified line-widths below 30 GHz. Additionally, dye lasers may have severe pulse-to-pulse longitudinal mode fluctuations [38, 39] complicating the calibration factor in single-shot measurements as the value of the overlap function changes from pulse-to-pulse. For averaged measurements the laser profile envelope becomes repeatable and the overlap function may therefore be quantified. In the saturation regime the line-width of the laser and internal mode structure is less important as long as every pulse is saturating the fluorescence.

Thanks to the well-controlled tunability of ECDLs the absorption line shape can be well characterized allowing for the overlap function to be calculated, Equation 2.10. In fixed wavelength TLAF the line shapes of the two transitions of the temperature marker are measured before every measurement by performing an excitation scan in the flame while simultaneously recording the laser wavelength. The lasers are thereafter tuned to the peak of the absorption line shape when the measurements are conducted. The overlap function is calculated with the information of the laser wavelength in combination with knowledge of the line shape.

In Paper III - V narrow-band lasers, in the form of ECDLs, were kept at fixed wavelengths for TLAF temperature measurements. The temperature was evaluated by comparing the ratio of the measured fluorescence signals $R_{exp} = \mathrm{F_a}/\mathrm{F_b}$ to a simulated ratio R_{sim}. The simulated ratio is given by:

$$R_{sim}(T) = \frac{\mathcal{L}_{23}(\lambda_{23}, T) \cdot f_2(T) \cdot B_{23}}{\mathcal{L}_{13}(\lambda_{13}, T) \cdot f_1(T) \cdot B_{13}} \tag{2.16}$$

where $\mathcal{L}$ is the overlap function, f the Boltzmann distribution and B the Einstein coefficient for stimulated absorption. The subscripts denote the involved levels, 3 being the excited

level and levels 1 and 2 the two ground states. The simulated ratios for gallium and indium are shown in Figure 2.6 when the lasers are locked to the peak of the absorption profiles.

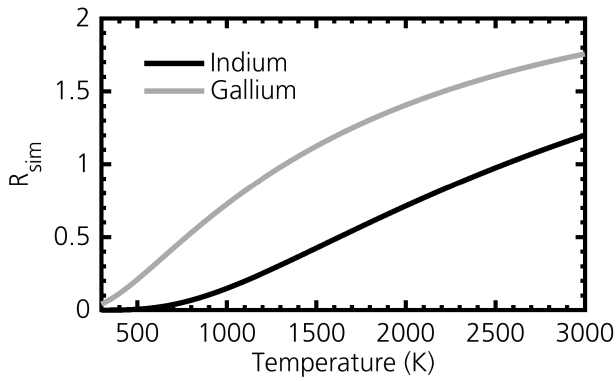

Figure 2.6: The simulated ratio according to Equation 2.16 when the lasers are tuned to the peak of the absoprtion profiles.

In the fitting of the excitation scans the following parameters are determined: temperature, reference collisional broadening, amplitude and wavelength shift. For subsequent simulations of R_{sim} the reference collisional broadening and wavelength shift are kept fixed from the values obtained through the fitting of the excitation scan. For measurements with fixed narrow-band lasers the accuracy of the evaluated temperature is affected by how well the simulated line shape is able to reproduce the actual line shape at different temperatures and conditions. The reference collisional broadening and wavelength shift are crucial for how well the simulated line shape reproduces the actual line shape and uncertainties in these parameters from the excitation scan will affect the accuracy of the measured temperature, discussed more in the next section.

If the measurement situation allows for line shape resolved TLAF to be performed in terms of experimental equipment and temporal resolution it should be preferred over fixed wavelength TLAF. This is because information of the line shape is provided in the line shape resolved measurement, thus no excitation scan is necessary and the errors related to the calculation of R_{sim} is avoided. Line shape resolved TLAF is, however, restricted to fast detectors, requiring the use of high-speed cameras for two-dimensional measurements whereas fixed wavelength TLAF can be performed with ordinary CCD cameras.

2.3.8 TLAF Error Sources

The figures of merit for any thermometric technique are the accuracy and precision of the temperature measurements. The accuracy determines how well the technique measures

the real value and the precision determines the spread of the measurements around the mean value. The errors affecting the accuracy and precision associated with the two TLAF techniques presented above will be discussed in the following section.

The accuracy of the technique is reduced by systematic errors which can sometimes be difficult to detect and quantify. The common systematic errors for line shape resolved and fixed wavelength TLAF are erroneous values of the Einstein A coefficients, inaccurate quantification of the laser powers and for two-dimensional measurements the beam profile compensation. Fixed wavelength TLAF has mainly two additional systematic errors: *i*) wavelength shifts from the peak of the absorption profile; and *ii*) inaccurate line shape simulations. The ratiometric method of TLAF reduces the systematic error from certain sources as it is the ratio of two values that are of interest and not the absolute values. For example the induced error due to an offset in the measured laser powers is reduced due to the ratiometric approach.

For the Einstein A coefficients only the ratio between the two coefficients is needed and not the absolute values, see e.g. Equation 2.11. Burns et al. [40] estimated the error of this ratio to ≈ 3 % for indium and estimated to contribute to a temperature error of 30 K at a flame temperature of 1800 K.

The quantification of the laser power during a measurement is one of the largest error sources in the TLAF technique. In the papers included in this thesis, a photodiode calibrated with a power meter has been used to measure the laser power during the measurements. The choice of power meter is important to improve the accuracy of the measured temperatures. A thermopile-based power meter is preferred over a photodiode power meter as it offers a flat spectral response, thus reducing the error due to the wavelength difference between the two lasers. Just as for the Einstein A coefficients it is the error of the ratio between the two laser powers that is of interest and not the absolute value. The relative error is expected to be lower then the specified uncertainty of the measurement value and in the included papers the error have been estimated to 2 %. This results in a temperature error of 1.5 % at flame temperatures.Errors in the beam profile compensation has the same effect as errors in the measured laser power, i.e., a beam compensation error of 2 % results in a temperature error of 1.5 %.

In fixed wavelength TLAF the temperature error due to errors of the fitted parameters, reference pressure broadening and wavelength shift, is quantified by investigating their effect on the temperature evaluation. This is done by changing the value of the fitted parameter and comparing the evaluated temperature to the temperature if the parameter was left unchanged. In Figure 2.7a the temperature error due to a wrongly assumed reference pressure broadening and wavelength shift is shown. For the reference collisional broadening the

true value has been assumed to be 6 GHz, in the same order as measured by Burns et al. [34] in a methane/air flame. A temperature error of approximately 1% is estimated if the real reference collisional broadening is 1 GHz off the assumed value.

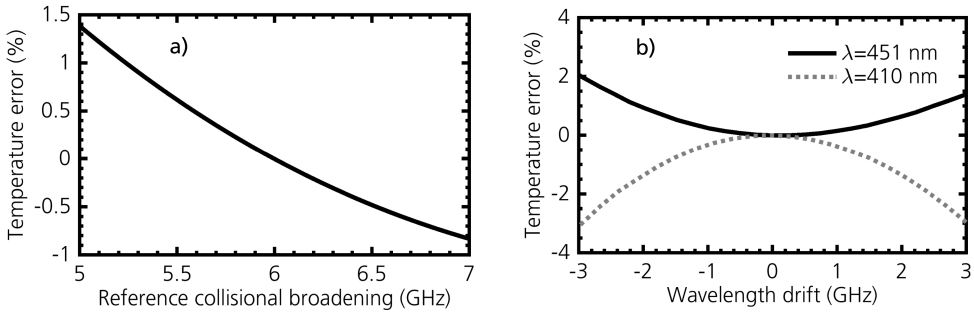

Figure 2.7: The simulated percentual temperature error resulting from an error in a) the reference collisional broadening and b) a wavelength shift.

In fixed wavelength TLAF the lasers are tuned to the peak of the absorption profile during the measurements and the accuracy is reduced if the laser is off the assumed peak position. There are several sources that may cause the laser to be off the peak: It may a drift due to a lack of stability of the laser, or more systematic errors such as an error in the fitting of the calibration line shape or a temperature-dependent pressure shift. All of the wavelength related errors manifests in the same way, although, the shift due to pressure difference happens simultaneously for both excited transitions. The temperature error as a function of wavelength being off the peak is simulated for the two transitions of indium at T = 2000 K and is presented in Figure 2.7b. The sign of the temperature error is different for the two transitions due to the ratiometric approach. This mitigates some of the errors, e.g. if both lasers were 3 GHz off the peak the maximum temperature error would be 1[illegible]%.

Additional complexities arise in measurements where the pressure varies, such as in internal combustion engines. The pressure shift can in principle be compensated if the pressure-shift was known and the pressure curve was measured simultaneously in the measurement. Eberz et al. [41] has investigated and quantified the pressure-shift of the $5P_{1/2} \rightarrow 6S_{1/2}$ transition of indium with nitrogen and other noble gases at pressures up to 450 mbar. Extrapolation of the reported data yields a frequency shift of 2 GHz/bar at 1500 K.

2.4 Concentration Measurements

Measurements of the absolute concentration of the seeded species is easily realised with narrow line-width diode lasers. The concentration measurements can be conducted simul-

taneously with the temperature measurement at the small additional cost of a photodiode located after the flame to monitor and measure the seeding levels. The photodiode measures the laser power without seeding, I_0, and with seeding I and the absorption of the seeded species can be calculated as $\alpha_\nu = I/I_0$. The concentration is derived from Beer-Lambert's law, yielding the number density N of the absorbing species as:

$$N = \frac{\ln(\alpha_\nu)}{\sigma(\nu)l} \tag{2.17}$$

where σ is the absorption cross-section and l the absorption path length. The absorption cross-section is related to the Einstein A coefficient as:

$$\sigma_{3i}(\nu) = \frac{A_{3i}\lambda_{3i}^2 g(\nu - \nu_0)}{8\pi}\frac{g_3}{g_i} \tag{2.18}$$

where $g(\nu)$ is the normalized line shape function, g_i the degeneracies and λ the wavelength for transition $i \rightarrow 3$.

Chapter 3

Experimental Equipment

Crucial for TLAF measurement is the use of a suitable light source for excitation of the seeded atomic species. The laser is unmatched in this category as it offers features that no other light source can contend with. The laser delivers collimated light with high photon fluxes and allows for tailoring of parameters such as wavelength, temporal pulse length and line width to the task at hand to provide the optimal light source.

In this chapter the experimental equipment of special interest for the work presented in this thesis is described, both the light sources used for excitation of the atomic species as well as the seeding system introducing the atomic species to the flame.

3.1 External Cavity Diode Laser

External cavity diode lasers (ECDL) have been extensively used throughout the work presented in this thesis, from acquiring atomic distributions and concentrations in Paper I, performing temperature measurements in Paper II through V to providing the seed light for the injection seeding of the OPO mentioned in Section 3.2. It is thus noteworthy to give a brief description of the working principle of the ECDL with its advantages and limitations.

The first demonstration of ECDLs is credited to MacAdam et al. [42] and Ricci et al. [43]. In its most simple form the ECDL consists of a laser diode and a diffraction grating, see Figure 3.1. The two surfaces of the laser diode forms an internal cavity where, generally, the end surface is highly reflective and the front surface, where the laser beam is emitted, has a lower reflectivity. An external cavity is established by aligning the diffraction grating at an angle in front of the laser diode so that the first order diffracted light is reflected back

into the laser. The feedback of the reflected light from the grating is greater then the internal feedback so that the emitted wavelength is governed mainly by the grating. ECDLs are made tunable by allowing the angle of the grating to be turned with piezo electronics. However, due to the competition between the internal and external modes there are sometimes, so called, mode hops where the wavelength jumps instead of continually changing with the grating angle. To reduce the occurrence of mode jumps and maximize the tuning range when tuning the grating angle the injection current can be adjusted simultaneously with the grating angle in a proportional way so that the internal laser modes also changes. The drawback is that the output power changes considerably during wavelength tuning.

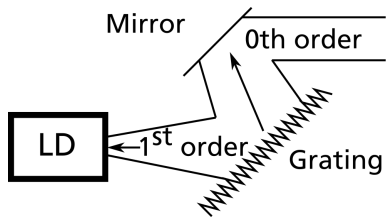

Figure 3.1: The simple configuration of an ECDL. The first order diffracted light is reflected back into the laser diode (LD) for external feedback and the zeroth order is emitted as the laser beam.

In the work presented in this thesis, ECDLs of model DL100 and DL100Pro (Toptica) were used. The specified linewidth of these models is below 1 MHz, which in combustion applications, with Doppler and pressure broadening, can be considered almost as narrow as a delta function. The output power is around 5 mW and the tuning range is up to 30 GHz, making it possible to scan most of the hyperfine structure of indium at flame temperatures [44]. Thanks to the large transition cross-section of atomic species it is possible to perform imaging experiments in combustion environments even with these relatively low laser powers as the laser-induced fluorescence (LIF) is very strong.

The wavelength of the ECDLs can be tuned or be kept fixed during an experiment, see Section 2.3.5. The output frequency of the laser can be stabilized either passively or actively. In the passive case the laser is set to the desired wavelength and the stability of the laser determines the frequency drift. The drift was investigated for the ECDLs mentioned above and it was found that the drift over the duration of ten minutes was small compared to the broad absorption lines, see Figure 3.2.

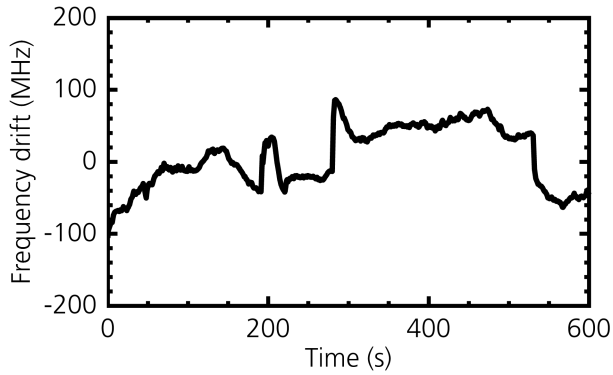

Figure 3.2: Frequency drift of an external cavity diode laser without active stabilization.

Active frequency stabilization or frequency locking is an established field of research often used in areas such as laser cooling and laser trapping. The basic idea of frequency stabilization is to generate an error signal when the laser drifts from the desired wavelength and then adjust the wavelength of the laser to the desired output. There are a multitude of techniques available for frequency stabilization [45–48]. For the temperature measurements in Papers III and IV the laser wavelength was kept fixed and two frequency locking schemes based on polarization spectroscopy and wavelength modulation spectroscopy were investigated. In conclusion it was found that there was no benefit in using either of these locking schemes compared to the passive alternative due to mainly three reasons. *i*) The stability of the non-stabilized lasers was already good, *ii*) the frequency-locking only allowed for corrections of the laser wavelength greater than 100 MHz and *iii*) the frequency stabilization complicates the experimental setup and requires a laser beam of considerable intensity which reduces the available laser power for the fluorescence measurements. Thus, for the fixed wavelength TLAF the passive frequency stabilization scheme was chosen.

3.2 Optical Parametric Oscillator

Instantaneous temperature measurements requires laser pulses with temporal pulse widths much shorter than the characteristic time scales of the combustion process and are often realized with nanosecond pulsed lasers. Pulsed laser sources able to provide light at the required wavelengths for probing the TLAF temperature markers can be either dye lasers or optical parametric oscillators (OPO). Both of these laser sources may experience large pulse-to-pulse fluctuations of the longitudinal modes and introduce considerable errors for evaluation of the overlap function between the laser line width and absorption profile. The overlap plays, as discussed earlier, an important role in the evaluation of temperature in

TLAF. This is why considerable amount of work of this thesis was invested in the development a tunable single longitudinal-mode optical parametric oscillator (SLM OPO) to be used for TLAF, although, also of great interest in high resolution spectroscopy. In TLAF a SLM OPO would allow for potentially higher LIF signal strengths, better knowledge of the overlap function, less pulse-to-pulse fluctuations and single-shot temperature measurements.

An OPO uses the process of parametric amplification in a pumped non-linear crystal to produce tunable laser light. The parametric amplification is governed by the interaction of three electromagnetic waves in a non-linear medium through the electrical susceptibility, χ^n, of the medium. In crystals, used both in optical parametric amplifiers (OPA) and OPOs, it is the second order susceptibility that is exploited. In the parametric process, two laser beams of wavelengths λ_2 and λ_3 are generated when the crystal is pumped with a laser of wavelength λ_1. The law of energy conservation dictates that $\frac{1}{\lambda_1} = \frac{1}{\lambda_2} + \frac{1}{\lambda_3}$ where the shorter wavelength of λ_2 or λ_3 is called signal and the other wavelength called idler. There is also a phase matching criteria $\Delta k = k_1 - (k_2 + k_3)$, k being the wave vectors, needed to be fulfilled to achieve parametric amplification.

In the general parametric amplification process the first signal and idler photons are generated from parametric noise (vacuum fluctuations) in the crystal [49]. If the photons satisfy both the energy conservation law and the phase matching criteria the amplification process is initiated. Macroscopic amplification is achieved as the spontaneously generated photons pass through the crystal increasing the emission of photons matching this wavelength. A higher amplification can be achieved in an OPO by placing the non-linear crystal inside a resonator where several round trips of either the signal or idler or both amplifies the laser light. Contrary to ordinary lasers the OPO works not by the creation of a population inversion and stimulated emission but instead the gain is provided by the pump pulse and only during the presence of a pump pulse is there amplification. The OPO configuration also restricts the signal and idler wavelengths to modes that are matching the cavity. Due to the randomness of the initially generated photons and that several longitudinal modes can be amplified, pulse-to-pulse fluctuations of the internal mode structure can be quite severe in OPOs [50]. The fluctuations can induce large errors in quantitative measurements sensitive to the overlap between the laser line shape and absorption line profile. This overlap is, as shown in Section 2.3.5, crucial for accurate temperature measurements in TLAF. Another disadvantage of the OPO is that the mode envelope is generally large due to the leeway in the phase matching criteria allowing many possible combinations of signal and idler wavelengths. To combat the problem of large mode fluctuations the OPO can be injection seeded. During injection seeding the initial photons are not generated by parametric noise but are instead provided by a secondary light source that has a narrow bandwidth. If in-

jection is successful only a single longitudinal mode, matching the injection light, should be lasing. Thus, the stabilization of the OPO output to a single longitudinal mode reduces both the threshold of the OPO as well as making it narrowband. The first successful demonstration of a frequency stabilized OPO was conducted by Bjorkholm et al. [51] with a cw Nd:YAG seed laser. Since then there have been many successful displays of frequency stabilized and SLM OPOs/OPAs through injection seeding e.g., [52–56].

A commercially available OPO (premiScan MB, GWU) with a linear cavity configuration was employed for the development of an injection seeded OPO. The OPO was pumped with the third harmonic of an injection seeded Nd:YAG laser with pulse energies approximately 90 mJ/pulse and 10 nanoseconds long. The unseeded OPO provides pulses with an energy of 30 mJ/pulse and with a specified spectral bandwidth of 120 GHz. The OPO was mounted with a BBO crystal allowing for signal wavelengths between 410 and 530 nm to be generated. The seeder was an external cavity diode laser, described more in detail in Section 3.1, with 5 mW output power and a specified linewidth of less than 1 MHz. A schematic of the seeding setup is displayed in Figure 3.3, including a simplified layout of the OPO cavity. The pump beam is directed into the cavity with the use of two mirrors mounted in a periscope configuration. These periscope mirrors are highly reflective for the pump wavelength at 355 nm and has high transmittance for the signal and idler wavelengths. In this work the seeder wavelength was chosen to match the signal.

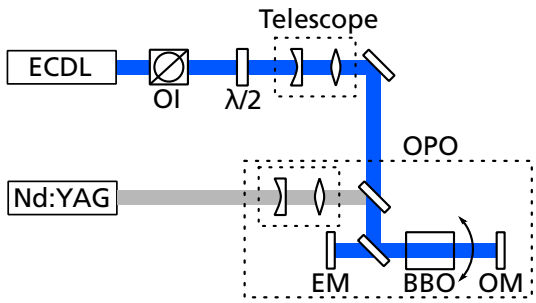

Figure 3.3: The optical setup of injection seeding of a linear cavity OPO. OI - optical isolator, λ 2 - half-wave plate, EM - end mirror, OM - output mirror.

Two different optical setups were used to couple the seeding light into the OPO cavity, *i*) seeding through the periscope mirror and *ii*) seeding through the end mirror. The best results were achieved when seeding using the first method and the following results are all recorded with this type of seeding arrangement. In this optical arrangement the seeding beam was first passed through two optical isolators, a necessity when using linear cavity OPOs due to the back-reflections to both the pump source and the seeding laser. After passing through the optical isolator the polarization of the seed laser was rotated with a

$\lambda/2$-plate to match the polarization of the signal beam. A telescope consisting of two lenses shaped the seeding beam to match the size and convergence of the signal beam.

The response of the OPO signal was characterized when seeded and unseeded in a wide variety of ways. The temporal repsonse of the OPO pulses was recorded on a photodiode. The response of the photodiode is shown in Figure 3.4 and it is observed that the build-up time decreases noticeably during seeding, as previously observed by, e.g. Raymond et al. [57]. Monitoring the build-up time during OPO operation may thus be a good indicator for controlling the performance of the seeding. The laser power is also seen to increase for the seeded OPO which is verified by a power meter. In Table 3.1 the average power of 500 pulses is presented for three different pumping power regimes, low, medium and high power. The low pumping power is near the OPO threshold. The power increases dramatically when seeding at lower pump powers and just at the threshold there is a seven-fold increase in power for the seeded OPO. This effect decreases as the pump power increases. The pulse-to-pulse variation in laser power is decreasing for the seeded OPO as shown by the percentual standard deviation in parenthesis in Table 3.1.

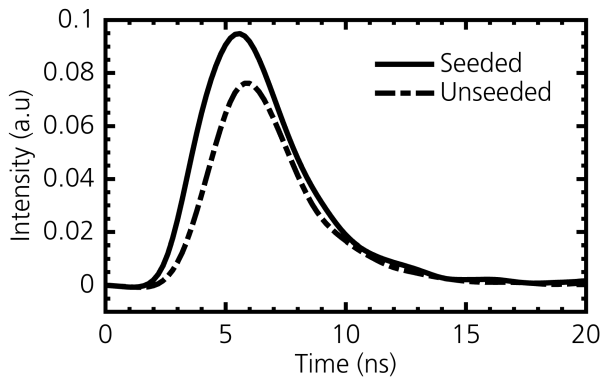

Figure 3.4: The build-up time of the signal beam for the seeded and unseeded OPO. The build-up time decreases and the intensity increases during successful seeding.

Table 3.1: The average output power of the OPO for 500 pulses when seeded and unseeded for three different pumping power regimes. The number in parenthesis is the percentual standard deviation.

	Output power (mJ)	
Pump Power Regime	Seeded OPO	Unseeded OPO
Low	0.29 (30%)	0.04 (30%)
Medium	0.73 (16%)	0.18 (30%)
High	2.18 (9%)	1.06 (13%)

The line width of the seeded OPO was measured with a confocal Fabry-Perot etalon with a free spectral range (FSR) of 1 GHz. The seeder was kept at a fixed wavelength while the etalon was scanned at rate of 0.1 Hz over a range of approximately 2.5 GHz to capture two peaks per scan. Etalon traces for the three pumping power regimes previously mentioned are shown in Figure 3.5 together with a fitted Gaussian curve. There is no noticeable difference in the linewidth for the three pumping regimes. The average full-width half-max (FWHM) for the three fits is 150 MHz which is considerably narrower than the unseeded OPO of 120 GHz. The seeded OPO is close to the Fourier transform limited linewidth which for a pulse length of 5 ns is 44 MHz.

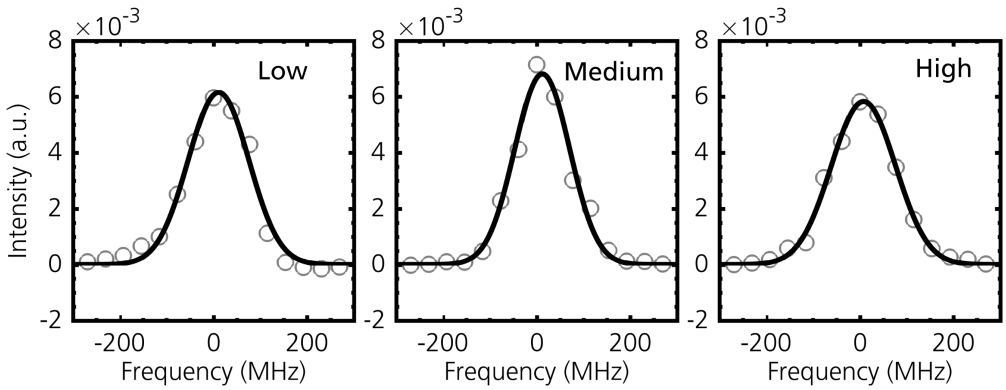

Figure 3.5: Etalon trace of the seeded OPO linewidth for three different pumping power regimes. The FWHMs are for the different power regimes, *Low* = 152 MHz, *Medium* = 137 MHz, *High* = 161 MHz.

The wavelength stability of the OPO when seeded was quantified with the use of a wavemeter and is shown in Figure 3.6. The OPO was seeded at 486 nm in the beginning of the measurement and the output wavelength is seen to be very stable. After 22 s the seeder laser was blocked and the frequency output of the "free-running" OPO starts jittering severely. The width of the frequency jitter can be considered to be analogous to the OPO gain profile and the seeded wavelength is observed to be at the edge of the jitter. This means that the seeding wavelength does not need to be in the centre of the OPO gain profile for successful seeding to be accomplished. This conclusion was further verified by scanning the seeder wavelength and not adjusting anything in the OPO. For these measurements, the wavemeter was aligned to only trigger when the OPO was seeded and, as shown in Figure 3.7, successful seeding was acquired over a range of wavelengths. The OPO was only seeded successfully at certain wavelengths, presented by the data points, even though the temporal resolution of the wavemeter is not a limitation. The frequency difference between sequential data points corresponds to the free spectral range of the OPO cavity.

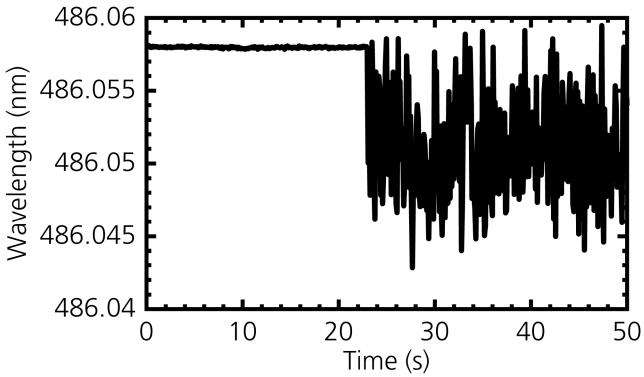

Figure 3.6: Frequency stability of the OPO for the seeded and unseeded case recorded on the wavemeter. In the beginning the OPO was seeded and around 22 s the seed laser was blocked.

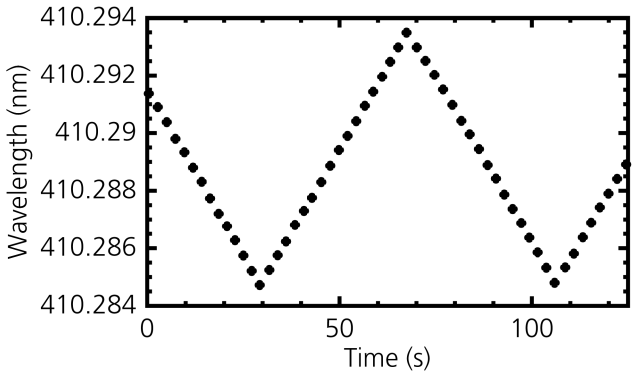

Figure 3.7: OPO output wavelength measured with the wavemeter when the seed laser was scanned. The wavemeter was triggered only when the OPO was seeded.

A draw back of the OPO is the limited quality of the spatial beam profile. The beam profile was characterized during injection seeding and it was observed that only the intensity in parts of the beam was increased during successful seeding. This indicates that only parts of the beam are narrow-band and experimental measurements would thus be difficult to conduct. This requires more research and further discussed in Chapter 5.

3.3 Multi-jet Burner

In laboratory experiments the choice of burner is of special interest for laser-based combustion diagnostics. The burner should provide a reproducible combustion environment to

allow for scientific studies of the physical properties under investigation and in the optimal case be able to decouple different physical phenomena to simplify the evaluation. For this reason there has been a large number of burners developed, from studying turbulent interactions in low-swirl burners [58, 59] to validation and development of detailed chemical kinetics in, e.g. heat-flux burners [60]. In Paper v a multi-jet burner was developed to provide one-dimensional flat flames with multiple variable parameters such as equivalence ratio, flow rate for pre-mixed and diffusion flames. The burner was later adopted for the temperature measurements presented in Papers iii and iv.

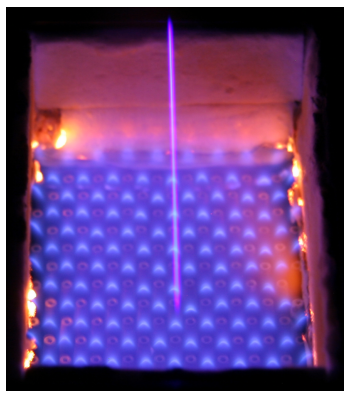

Figure 3.8: The multi-jet burner with a stoichimetric mixture of methane and air. A laser beam visualizing the laser induced fluorescence of indium is observed above the small jet flames.

The multi-jet burner, seen in Figure 3.8, consists of two separate plenum chambers, one chamber connected to 181 individual jets and one chamber providing a co-flow through a perforated plate around the jets. The 181 jets are distributed in an area of 60 mm x 100 mm surrounded by a water cooled jacket and shield rings to produce a uniform rectangular burned gas region of 70 mm × 40 mm. The burner design allows for both diffusion and pre-mixed flames with temperatures ranging from 1000 K to 2000 K. Additives in the form of gases or liquid droplets can be seeded to the flame for quantitative studies on the additives effect on the combustion process. The burner design also allows for detailed investigations of burning particles such as biomass pellets.

3.4 Atomic Seeding Systems

The seeding of the atomic species into the combustion environment is crucial for TLAF and for this end various seeding techniques have been developed. The first TLAF meas-

urements, realized in the 1970s by Omenetto et al. [61] and Haraguchi et al. [62], used a so called nebulizer system and has since been used extensively in many TLAF applications [27, 44, 63, 64]. In the nebulizer system a metallic salt, e.g., $InCl_3$ or In_2O_3, is dissolved in a liquid (solvent) and introduced through a capillary tube into a nebulizing chamber as droplets. The droplets are reduced considerably in size through various methods and in the optimal case forms a very fine mist of metal halides that is carried by the gas flow to the flame where, upon passage through the reaction zone, the halides are atomized. However, the droplets are often split into a range of sizes and large droplets not carried to the flame needs to be drained from the system to prevent clogging which complicates the experimental arrangement. Additionally the seeding concentration may vary severly during a measurement which, depending on the measurement, will introduce large errors. The solvent have also been observed to change the flame chemistry and the combustion behaviour [65–67]. Nevertheless, there are some reports indicating that a correctly handled nebulizer system may have negligible effects on the flame properties [68].

Manteghi et al. [23] have demonstrated a novel seeding concept using a modified PIV system with a vibrating fluidized bed containing $InCl_3$ salt and Al_2O_3 particles. This method avoids solvent effects on the flame chemistry. An optically based seeding technique demonstrated by Medwell et al. [69, 70] also circumvents solvent effects on the flame properties. In this optical method, laser ablation of a rotating indium rod produces atoms and agglomerates that are carried to the flame producing free atoms after the reaction zone. This method requires the use of a powerful laser for the ablation.

In Paper I a seeding system was developed to avoid solvent effects and allow for greater flexibility regarding the type of burner used. The seeding system, described below, was successfully used in Papers II - V.

3.4.1 Bubbler System

The main component in the seeding system developed in Paper I is a bubbler containing an organometallic substance with the atomic species to be seeded to the flame. This type of bubbler is often used in the field of solid state physics, e.g. in metalorganic vapour phase epitaxy (MOVPE). For the elements of interest for TLAF, i.e. Group III metals in the periodic system, the organic component is three methyl groups connected to each metal atom, i.e. trimethylindium (TMI) or trimethylgallium (TMG). The first and, as far as the author know, only use of a seeding system based on an organometallic substance for TLAF measurements was reported briefly by Tian et al. [71].

During the construction of the seeding system safety concerns have to be addressed as the organometallic substance presents some hazards and risks. For instance, TMI melts at

88°C and starts to decompose above 140°C. It has a pyrophoric behaviour and for thermal decomposition, an autocatalytic behaviour has been reported. The toxicity of the trimethyl compounds have not been assessed properly but skin and eye burns as well as respiratory irritation may be caused by exposure to the substance. The design is also of consideration for the performance of the seeding system in terms of stability and temporal response of the seeded concentration.

In the bubbler, sublimation of the organometallic substance due to the high vapour pressure saturates a carrier gas flowed through the bubbler. The carrier gas must be inert to not react with the metalorganic and in the work presented in Papers I - V nitrogen was used as the carrier gas. It is also possible to use hydrocarbon gases such as methane as the carrier gas [71], which might prove useful in experiments with diffusion flames as no nitrogen have to be added to the fuel, although, the carrier flow may often be neglected due to the small amount needed. Usually the carrier flow is in the order of 0.05 litres per minute. The bubbler is located in a chiller bath that allows for accurate control of its temperature. The seeding concentration can be adjusted by either changing the temperature of the bath or amount of gas flow through the bubbler. To reduce the risk of contaminating the bubbler with trace amounts of water or oxygen the seeding system was designed to be able to be evacuated by a vacuum pump before each measurement. A schematic of the seeding system is shown in Figure 3.9.

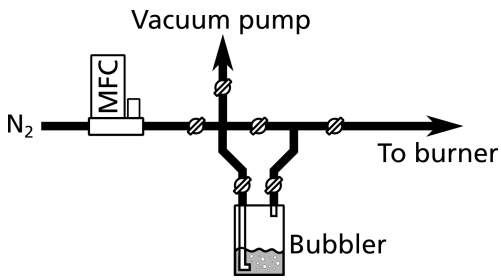

Figure 3.9: Schematic of the seeding system. Nitrogen, controlled by a mass-flow controller, is flowed through the bubbler by adjusting the valves. Contamination of the seeding system is prevented by vacuating the gas tubes of any gas using the vacuum pump while having the bubbler closed.

Two organometallic substances have been used to for TLAF, TMI in Papers I - III and TMG in Paper III and IV. The vapour pressure of the two substances is given by Equation 3.1 with the constants for each substance presented in Table 3.2. In practice this means that TMG has a higher vapour pressure and needs thus to be kept at a lower temperature than TMI to have similar seeding concentrations.

$$log_{10}P(\mathrm{Pa}) = A - \frac{B}{T(K) + C} \tag{3.1}$$

Table 3.2: Parameters for the vapour pressure of the two organometallic substances seeded to the flame in Paper III.

Substance	A	B	C	Reference
Trimethylindium	13.10	3204	0	[72]
Trimethylgallium	27.45	5784	41.83	[73]

The response time of the seeding system was investigated by changing both the carrier flow rate and the bubbler temperature. The measurements were performed in the previously described multi-jet burner in Section 3.3 in a stoichiometric methane/air flame seeded with TMI. Two ECDLs were used to measure the absorption of the $5P_{1/2} \rightarrow 6S_{1/2}$ and $5P_{3/2} \rightarrow 6S_{1/2}$ transitions at 410 nm and 451 nm, respectively, of indium. As expected a change in carrier gas flow results in a much faster change of the seeding concentration than a change in bubbler temperature. This fast response in seeding concentration is advantageous when conducting measurements over a wide range of equivalence ratios as the indium signal decreases significantly in lean flames due to oxidation. In Figure 3.10 the response of the seeding system is shown for a few cases where the flow rate of the carrier gas is changed. The time response of the system is dependent on the length of the gas line and burner configuration.

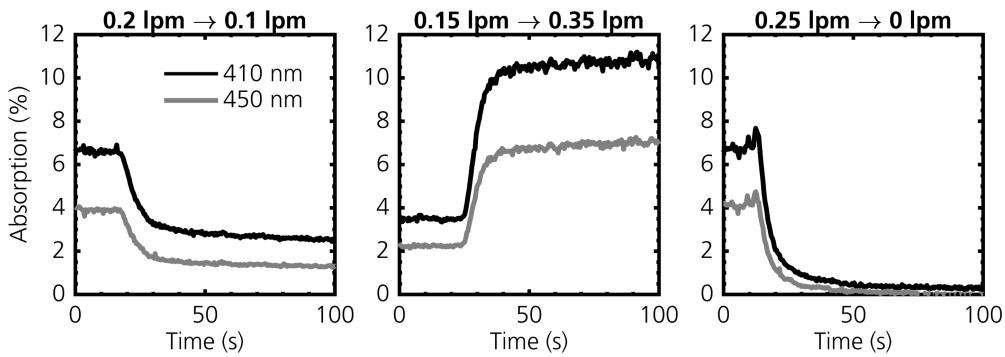

Figure 3.10: Response time of the seeding system for changes in carrier gas flow as noted above each chart (lpm = litres per minute). The measurements were conducted in the multi-jet burner presented in Paper V. After a change in gas flow a power law behaviour of the seeding concentration is observed moving asymptotically to the set point.

As seen in the right most chart of Figure 3.10, when the bubbler is turned off, there is

always a slight residual signal decreasing slowly with time. The residual signal is attributed to deposition of TMI/TMG or oxidized metals (In_2O_3/Ga_2O_3) along the tubing and in the burner. When the seeding is stopped some of the depositions continue to be released resulting in a very low concentrations of the atomic species in the flame. Nevertheless, no visible clogging effects have been observed due to the deposition even in porous plug burners of McKenna type. The first time a new burner and tubing is used with the seeding system a severe delay is observed between turning on the seeding and signal in the flame.

Chapter 4

Temperature Measurements

Temperature information is critical in a majority of combustion related research in, e.g., quantification of concentrations and development of chemical kinetic models. Accurate and precise temperature measurements are still highly demanded, thus the main work reported in this thesis has been on the development of diode-laser-based two-line atomic fluorescence for thermometric measurements. Diode lasers, instead of more conventional pulsed nanosecond lasers, were chosen due to the beneficial features that are hard to realise for pulsed lasers. Diode lasers are more compact, can provide better wavelength control such as single-mode lasing and allows for simple implementation of simultaneous concentration measurements. These features are, however, obtained at the expense of instantaneous single-shot measurements due to the low peak power of diode lasers.

Diode-laser-based TLAF was first reported by Hult et al. in 2004 [28] and many displays of TLAF and OLAF was thereafter published by the aforementioned group. A majority of the work conducted throughout this thesis covers the development and extension of the diode-laser-based TLAF technique for a wide variety of applications. An overview of the thesis work is presented in the following sections of this chapter. In the first section the choice of atomic species for two-line atomic fluorescence and its implications are discussed. In Section 4.2 temperature measurements conducted at low pressure using the line shape resolved TLAF technique (see Section 2.3.6) are presented. Temperature measurements in atmospheric conditions are shown in Section 4.3, including measurements using a novel LIDAR-based (Light detection and ranging) setup, useful in situations with limited optical access. Temperature measurements in optically harsh environments are demonstrated in the last section of the chapter.

4.1 Temperature Markers for TLAF

The choice of atomic element as temperature marker determines the measurable temperature range and is important for the accuracy and precision of the evaluated temperatures for the TLAF measurements. The three elements that are most commonly considered for TLAF are: gallium, indium and thallium, ordered by increasing energy gap, ΔE, between the two lower ground levels. Information relevant for TLAF measurements for each of these elements is presented in Table 4.1. All elements are seen to have similar characteristics: the Einstein coefficients are all of the same order, almost all wavelengths are in the visible region and easily accessible with modern lasers. The largest difference between the elements is the energy gap between the two lower ground levels. This energy gap is also the main deciding factor when selecting the element to use, assuming differences in the seeding arrangement can be disregarded, as it determines the measurable temperature range and measurement precision.

Table 4.1: Relevant physical constants for the Group III metals used in two-line atomic fluorescence. Data retrieved from [74].

Atomic element	Energy gap (cm^{-1})	Transitions	Wavelength (nm)	Einstein A ($10^8 s^{-1}$)
Gallium	826.19	$4P_{1/2} \rightarrow 5S_{1/2}$	403	0.485
		$4P_{3/2} \rightarrow 5S_{1/2}$	417	0.945
Indium	2212.598	$5P_{1/2} \rightarrow 6S_{1/2}$	410	0.50
		$5P_{3/2} \rightarrow 6S_{1/2}$	451	0.89
Thallium	7792.7	$6P_{1/2} \rightarrow 7S_{1/2}$	378	0.625
		$6P_{3/2} \rightarrow 7S_{1/2}$	535	0.795

The population of a three-level system in thermal equilibrium is governed by the Boltzmann distribution and for all three mentioned elements only the two lower levels will be populated at flame temperatures and below. The relative population between these two levels is determined by the energy gap and temperature. Two competing process related to the energy gap determines the temperature range in which the element is usable. On the one hand there needs to be sufficient population of the upper ground level to achieve a good signal-to-noise ratios of the LIF signal, i.e. the energy gap should not be too big. On the other hand the precision is proportional to the reciprocal of the energy gap [27, 75], i.e. the energy gap should be as large as possible. There is thus a trade-off between these two processes that needs to be accounted for when choosing the temperature marker for a specific measurement situation.

The temperature sensitivity and population of the upper ground level is shown in Figure 4.1. The temperature sensitivity is defined as a change in ratio, see e.g. Equation 2.16, of the two

fluorescence signals per unit temperature. A smaller energy gap results in a higher temperature sensitivity at lower temperatures as observed in Figure 4.1 with decreasing sensitivity at higher temperatures. Gallium, with the smallest energy gap, reaches its peak sensitivity at 600 K while thallium with the largest gap is not sensitive below 3000 K. At flame temperatures indium and gallium have similar temperature sensitivities. As seen in right graph of Figure 4.1 the fractional population of the upper ground level limits indium to temperature measurements above 900 K due to the low population of level 2 at lower temperatures, even though indium shows sensitivity at these temperatures.

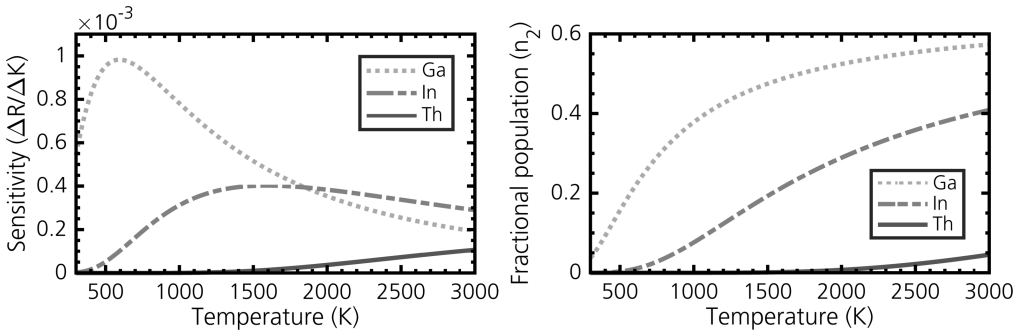

Figure 4.1: *Left* – Temperature sensitivity of the elements most relevant for TLAF, gallium, indium and thallium. *Right* – Fractional population of the upper ground level for the three atomic elements at different temperatures.

The first demonstrations of TLAF in the 1970s were conducted with both indium and thallium [61, 62]. Thallium was abandoned early due to its toxic nature and the low temperature sensitivity below 3000 K. Since then, the majority of TLAF papers have employed indium as the temperature marker due to its good sensitivity at flame temperatures and ease of seeding. Gallium was also discarded in favour of indium due to the lower precision at flame temperatures. However; in measurements where the temperature is expected to go below 1000 K gallium should perform better than indium. These lower temperatures are of interest in low temperature chemistry, such as in the initial injection stages of internal combustion engines and in plasma assisted combustion [76–78].

In Paper III, gallium is, for the first time, investigated as a temperature marker in TLAF. As a first assessment of the potential of gallium as a temperature marker measurements were conducted in a multi-jet burner (see Paper V) with temperatures ranging from 1500 K to 2000 K. Even though the temperature range in the multi-jet burner does not showcase the full advantage of gallium compared to indium, the multi-jet burner provides well-characterized and stable conditions in which to compare the different measurements. Spatially resolved

measurements in one dimension using fixed wavelength TLAF of gallium and indium were conducted in Paper III.

Atomic data for the two atomic elements used for the line shape fitting is presented in Chapter 5.1. The accuracy of the technique at flame temperatures was found to be independent of the atomic marker. A possible systematic error source that could cause a difference in accuracy for the two atomic markers is the width of the line shape. The hyperfine levels of gallium are more closely spaced than the indium levels. Nevertheless, the large broadenings from both the elevated temperatures ($\approx$ 1 GHz) and pressure ($\approx$ 5 GHz) results in a negligible differences in accuracy for example from laser drifts. The main errors affecting the accuracy comes from the technique itself and are not dependent on the atomic element used. The precision is, on the other hand, proportional to the inverse of the energy gap as previously mentioned and indium should theoretically have better precision at flame temperatures. In Figure 4.2 the combined signal-to-noise ratio for indium and gallium is presented together with the corresponding precision for equivalence ratios ranging from 0.8 to 1.3. The combined SNR is the sum of the SNR for the two TLAF transitions for each species. The SNR itself was calculated as the mean LIF signal divided by the standard deviation of the LIF in the flat temperature region of the flame. Analogously, the precision was determined from the standard deviation of the temperature profile in the same flat temperature region. It is observed that the SNR of gallium is higher than that of indium caused by differences in the experimental arrangement such as unequal seeding concentrations, peak filter transmissions and LIF collection optics. Even though indium has a lower SNR than gallium the precision is better due to the larger energy gap.

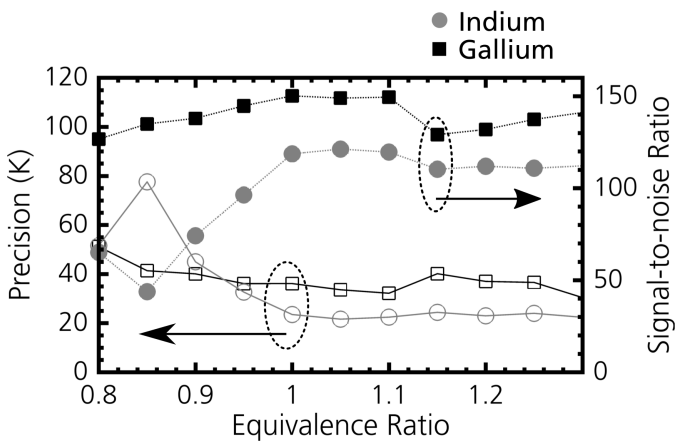

Figure 4.2: Precision (hollow markers) and the corresponding signal-to-noise ratio (filled markers) for gallium and indium for different equivalence ratios.

4.2 Low-pressure Temperature Measurements

Even though a large majority of combustion applications transipres at atmospheric or elevated pressures, e.g., in internal combustion engines or gas turbines, there is a substantial interest for combustion at lower pressures. The interest for combustion at lower pressures is due to changes in the dynamics of combustion resulting in features beneficial in for example detailed chemical investigations. As an example the reaction zone, normally characterized by steep gradients in both temperature and concentration profiles, becomes thicker at lower pressures. The increased thickness of the reaction zone allows for the gradients to be better resolved and can thus provide better data for model validation. Low-pressure combustion is a large research field for the development of detailed chemical kinetics [79–81]. Another application of low-pressure combustion is that of production of nanoparticles [82–84] and for all these applications information of the temperature is of great importance.

A problem in low pressure combustion environments is that many thermometric techniques that work well at atmospheric conditions suffer from the decreased number density at lower pressures. In Rayleigh scattering thermometry the already low signal at flame temperatures is decreased even further at low pressures resulting in very poor signal-to-noise ratios. Rayleigh scattering also suffers from interference from elastic scattering from surfaces in enclosed chambers such as low-pressure vessels, although, the use of structured planar laser illumination (SLIPI) might overcome such problems [85]. Another thermometric technique with a decreased usability in low-pressure environments is coherent anti-Stokes Raman spectroscopy (CARS). Not only is the signal strength proportional to the number density squared in CARS measurements, the measurements are often limited to point-wise measurements and the limited optical access might also restrict the use of CARS. Temperature measurements derived from excitation scans of seeded molecules such as OH [86] and NO [87] have been shown to provide accurate temperature measurements in low-pressure flames. However, the excitation scans are time consuming and requires the use of tunable pulsed lasers. There have also been reports that the seeding of NO might alter the flame chemistry [88]. Two-line atomic fluorescence has on the other hand good potential for providing accurate and precise measurements in low-pressure flames. Additional to the advantages discussed in earlier chapters, an even stronger fluorescence signal is expected at low pressures due to a decreased fluorescence quenching.

In Paper II development of diode-laser-based TLAF for imaging of the temperature distribution in a low-pressure flame is presented. A McKenna type burner placed in a chamber with a pressure of 50 mbar was seeded with indium using the seeding system described in Section 3.4.1. The burner was translated to different heights to map the temperature distribution of three flames running a methane/oxygen/nitrogen mixture of equivalence ratios

1.16, 1.42 and 1.63. The oxygen was proportionally increased in relation to the nitrogen for each equivalence ratio to keep the flame stable.

The fluorescence signal was recorded using an intensified high-speed camera when each of the exciting lasers were consecutively tuned over the two transitions of indium. The laser beams were formed into sheets, with a height of approximately 5 mm, and imaged on the high-speed camera, thus every pixel contained information of the line shape of each transition of indium. The experimental procedure is explained in more detail in Paper II. The LIF signal of a single pixel and single scan is shown in Figure 4.3. Together with the presented line shapes is the response of a Fabry-Perot etalon and laser power measured on a calibrated photo diode. The etalon, with a free spectral range of 1 GHz, measured the frequency scale of the wavelength tuning. As seen in the figure one scan for a single pixel provides good quality data that could be used to evaluate the TLAF temperature. However, as the time resolution is already limited due to the wavelength scanning and the flame is stable the line shapes were averaged over 10 scans to increase the signal-to-noise ratio.

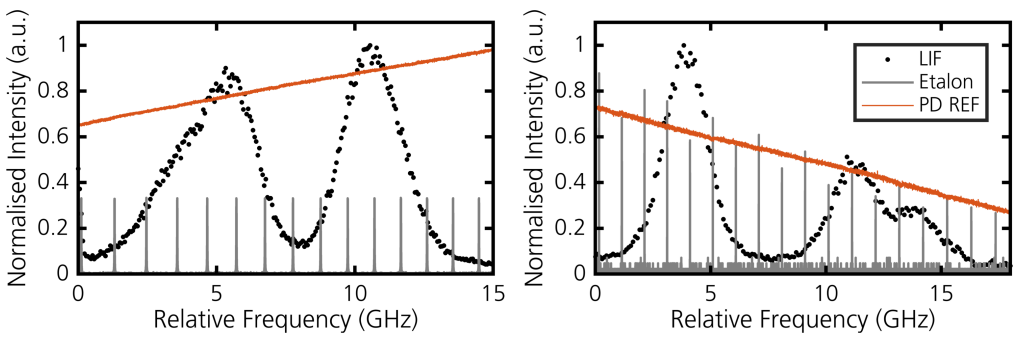

Figure 4.3: The recorded LIF signal (*black dots*) on a single pixel of a single scan for the two transitions of indium. The *gray line* is the fringes recorded on the etalon as the lasers were scanned. The laser power during wavelength tuning is shown as the *red line*. The left figure shows the $5P_{1/2} \rightarrow 6S_{1/2}$ transition and the right figure $5P_{3/2} \rightarrow 6S_{1/2}$

In Paper II, two-dimensional temperature distributions of the three flames with different equivalence ratios are presented. Temperatures were derived using the line shape resolved TLAF technique and these measurement are discussed in more detail in the paper. From the line shapes themselves it is possible to deduce the temperature as discussed in Section 2.3.4. In this technique, termed one-line atomic fluorescence (OLAF), the line shape is described by a unique combination of a Lorentzian and Gaussian broadening component. If the temperature dependence of the Lorentzian broadening component is known, see Equation 2.14, the temperature can be deduced from the line shape itself. Even though Paper II was focussed on temperature measurements using TLAF, the available data (wavelength

resolved line shapes) allows for OLAF temperatures to be evaluated from the fitting of the line shapes. The OLAF temperatures are independent of each other and of the TLAF measurement and may serve as cross-validation.

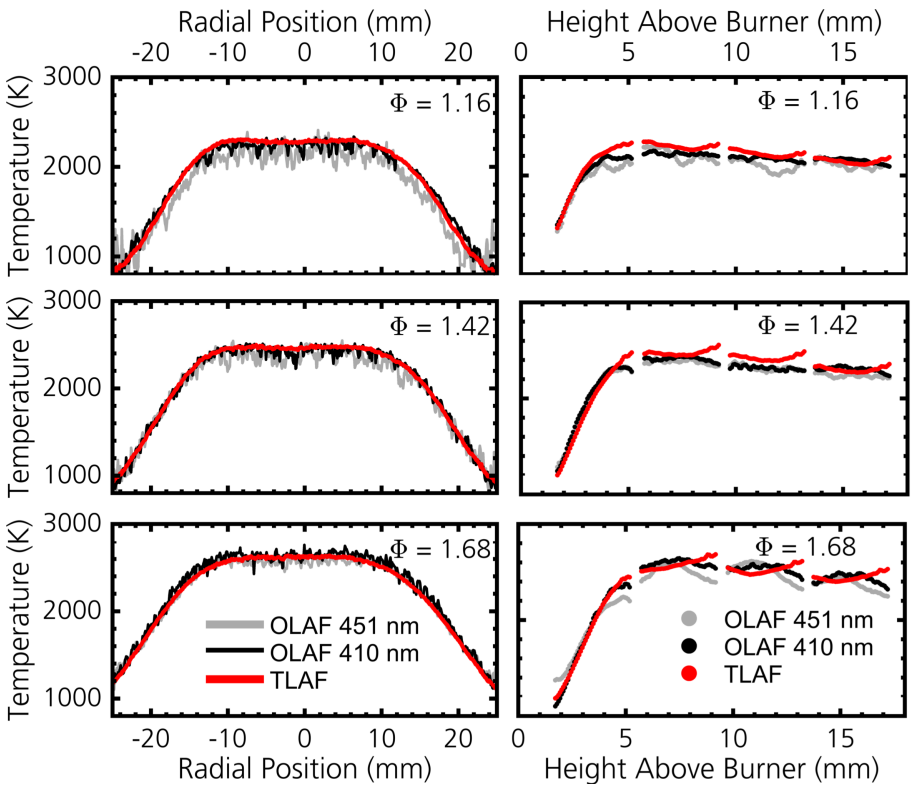

Figure 4.4: *Left column* – Horisontal temperature profiles for OLAF and TLAF at a height of 10 mm above the burner for the three flames. *Right column* – Vertical temperature profiles in the centre of the burner.

In Figure 4.4 vertical and horizontal temperature profiles for TLAF and OLAF are presented for the three flames. The vertical profiles are taken from a single pixel line at a height of 10 mm above the burner surface. The vertical profiles for each equivalence ratio measured with the different methods agree well with each other, although the OLAF temperatures have a little worse precision than the TLAF temperatures. The OLAF temperatures for the $5P_{1/2} \rightarrow 6S_{1/2}$ transition have a better precision than the $5P_{3/2} \rightarrow 6S_{1/2}$ transition. This is most likely due to the relatively simpler line shape of the $5P_{1/2} \rightarrow 6S_{1/2}$ transition with fewer hyperfine transitions that are more spaced, reducing the fitting complexities. The temperature profiles evaluated from the $5P_{3/2} \rightarrow 6S_{1/2}$ transition are seen to exhibit large variations at the edges of the flame where the temperature is around 1000 K and a low LIF

signal is expected due to the low population of the $5P_{3/2}$ level at these temperatures.

The vertical temperature profiles, shown in the right column of Figure 4.4, are calculated as the average temperature in the radial direction between -5 and 5 mm for each flame. Each horizontal profile consists of four separate measurements where the burner has been translated between each measurement. The TLAF and OLAF temperatures agree fairly well for all heights, even for the steep gradients in the reaction zone. The advantage of the OLAF evaluation compared to TLAF is the insensitivity to the beam profile compensation. In, e.g. the vertical profile of the $\Phi = 1.42$ flame, a slight curvature is observed in each segment for the TLAF measurements, attributed to the beam compensation, while the OLAF temperatures are all fairly flat. For the TLAF measurements the beam profile compensation introduces a temperature error of up to 2 %. This error is not present in the OLAF temperatures. However, the OLAF temperature is more sensitive to the SNR of the measured line shapes which in turn affects how well the line shapes can be fitted. For flames at higher pressures, such as atmospheric flames, the uncertainty in the OLAF measurements is possibly increased due to the Gaussian component becoming smaller than the Lorentzian component. Nevertheless, Burns et al. [34] have demonstrated OLAF thermometry in atmospheric flames and they found that certain parts of the hyperfine structure, the troughs between the individual hyperfine transitions, is sensitive to small temperature changes due to the drastic change in this trough structure even for small temperatures.

The accuracy of the OLAF temperatures depend on the SNR of the recorded line shapes. The SNR and its effect on the evaluated OLAF temperature was investigated for different parts of the flame. In Figure 4.5 two cases with different SNR are shown with the data points as black dots, the best fit for each line shape as the red line and the grey shaded area is the 95 % confidence interval for the fitting parameters. The SNR was calculated as the standard deviation of the fitted residuals divided by the peak signal strength and the SNR of each line shape is noted in the respective figure. The worst possible SNR is shown in the left column and a typical case is shown in the right column. The worst case scenario is recorded in a region of the flame that is close to the burner surface and/or on the edge of the burner resulting in a low fluorescence signal for the 451 nm transition due to both a low temperature and possibly a decreased seeding concentration. At this very low SNR the OLAF temperatures are not meaningful due to the large confidence interval of the fit but even so the fitting allows for the TLAF temperature to be evaluated. At the edges of, e.g., the leanest flame in Figure 4.4, it is seen that the TLAF temperatures follows a reasonable trend while the OLAF temperature of the 451 nm transition are noisy.

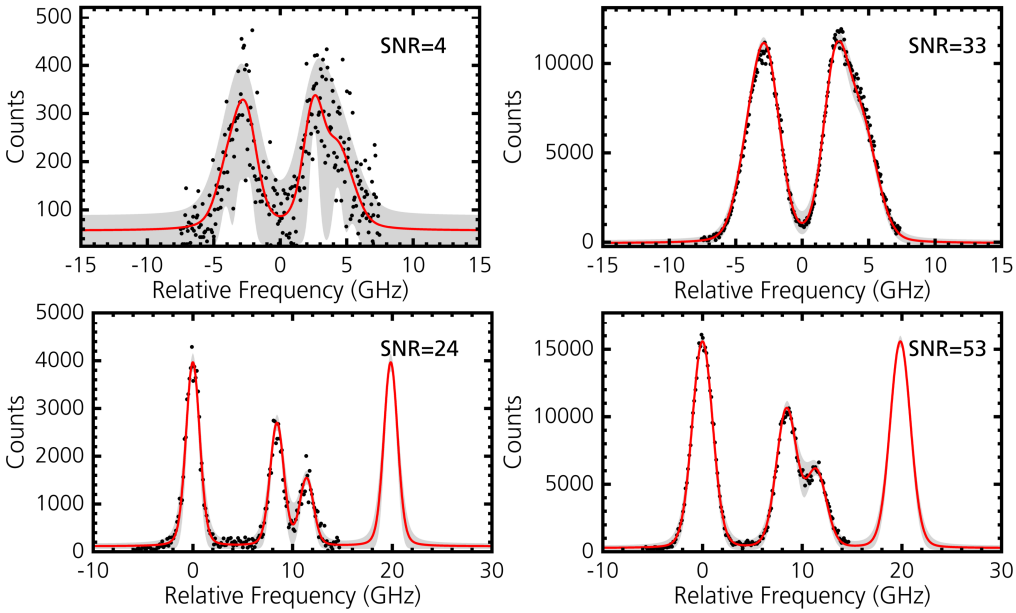

Figure 4.5: Examples line shapes with low (left column) and high (right column) SNR for the two selected transitions of indium. The $5P_{3/2} \rightarrow 6S_{1/2}$ transition in the upper two frames and $5P_{1/2} \rightarrow 6S_{1/2}$ in the lower frames. The SNR is stated in each chart. The red line is the best fit to the data points and the shaded area shows the 95% confidence interval for the fitting parameters. For good SNR the shaded area is hidden by the best fit.

The 95 % confidence interval of the fitted parameters is used as an indication of the sensitivity of the OLAF technique to the SNR. From the upper and lower bound of the confidence interval a percentual temperature interval is constructed. This interval is the difference between the upper and lower bound of the fitted temperature divided by the best fitted temperature. The percentual temperature interval is plotted against the SNR of the line shape in Figure 4.6. The 451 nm transition is seen to generally have a worse SNR than the 410 nm transition. This is mainly due to the low population of the upper ground state for all temperatures and especially at lower temperatures. A dependence between the SNR and temperature interval is observed and the temperature interval for the 451 nm transition matches that of the 410 nm for higher SNRs. It should be noted that this temperature interval does not translate directly to precision or accuracy of the technique. The precision and accuracy of the OLAF technique depends on several possible systematic error sources related to the simulation of the line shape, e.g., hyperfine spacing, relative intensities, exponent in Equation 2.14.

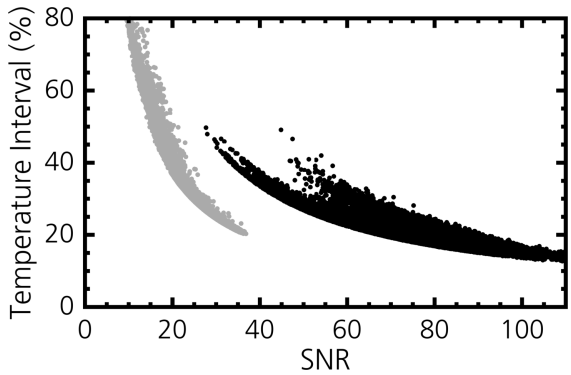

Figure 4.6: Temperature interval is defined as the difference between evaluated temperatures using the upper and lower bounds of the fitted parameters determined by the 95 % confidence interval. The temperature interval is here divided by the fitted temperature to show the percentual error as a function of the SNR of the line shape.

The absorption lines of the probed atom can be shifted in relation to a fixed reference wavelength due to two collisional-related shifts, either due to a difference in pressure or due to a number density-dependent shift. In laboratory flames, often kept under constant pressure, there is no pressure-induced shift as the pressures is approximately constant over the whole flame. The number density, however, varies with temperature and the line shape will thus be shifted depending on the temperature of the flame. The pressure shift is induced by the presence of molecules and atoms perturbing the energy levels of the probed atom, in this case indium and the magnitude of the perturbation is dependent on the interacting molecule, i.e. on the gas composition. A higher pressure or number density means that the probability of a molecule interacting with the emitting atom increases and the shift is increased. The number density-dependent shift will introduce errors in the temperature evaluation for fixed wavelength TLAF measurements where the laser wavelength is supposedly tuned to the peak of the absorption profile but not in these line shape resolved TLAF measurements conducted in the low-pressure burner.

The line shape resolved measurements in the low-pressure burner may instead be used to quantify the induced shift as line shapes for temperatures ranging from 900 K up to 2600 K are measured simultaneously, i.e. synchronized in time. The low temperatures are measured at the edges of the flame and higher temperatures in the centre as shown in Figure 4.4. By comparing the line shapes measured at all these temperatures the number density-dependent shift can be investigated from the wavelength shift parameter in the fitting procedure. The number density-dependent shift for the two transitions of indium, $5P_{1/2} \rightarrow 6S_{1/2}$ and $5P_{3/2} \rightarrow 6S_{1/2}$, is plotted against the reciprocal of the evaluated TLAF temperature in Figure 4.7. A linear relationship between the shift and the reciprocal tem-

perature is observed and the red line in the figure shows a linear fit to the data. The slopes of the two transitions at 410 nm and 451 nm is -161 MHz/1000 K and -166 MHz/1000 K respectively. The slope of the shift was found to be the same for all equivalence ratios even though the nitrogen volume fraction goes from 0.43 for the leanest flame to 0.16 for the richest indicating that this shift is somewhat independent on the gas composition.

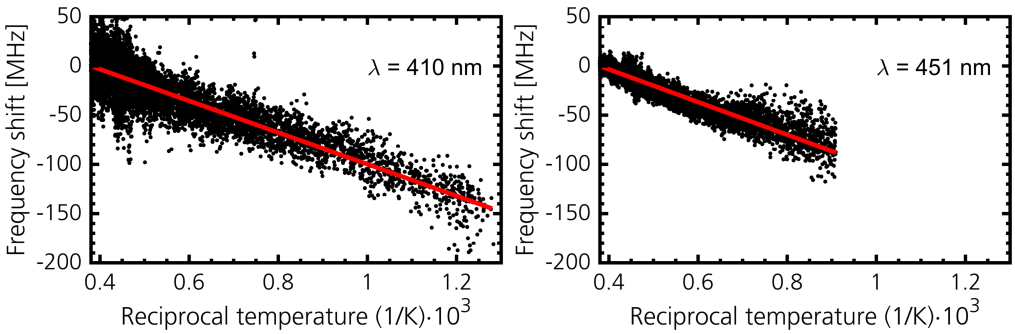

Figure 4.7: The relative shift of the two transtions of indium as a function of the reciprocal temprature. The left figure shows the pressure shift for the 410 nm line and the right figure the shift for the 451 nm line. The shift was evaluated from the fitting procedure (see text) and the temprature is the temperature evaluated from TLAF. The red line shows a linear fit to the data. Data below 1200 K has been omitted for the 451 nm transition due to the low SNR.

4.3 Atmospheric Pressure Measurements

For atmospheric temperature measurements the fixed wavelength approach was chosen both due to the limited scanning range of the lasers making it difficult to cover the whole line shape at atmospheric pressures (although not completely necessary) and to avoid the need for a high-speed camera when spatially resolved measurements are conducted. The fixed wavelength TLAF concept was evaluated in Paper III where measurements were conducted in the multi-jet burner and compared to rotational CARS measurements.

The experimental setup used for the fixed wavelength TLAF measurements is shown in Figure 4.8. Two diode lasers were aligned in relation to a chopper wheel to switch between the lasers during a measurement. Additionally the chopper was aligned so that both lasers were blocked at certain times. With the use of a camera synchronized to the chopper a sequence of three different images was acquired: a background when both lasers were blocked, and two images of the laser-induced fluorescence signal of the respective laser. This experimental procedure, shown in Figure 4.8b, compensates for slow fluctuations and drifts during meas-

urements such as varying seeding concentrations and slowly changing background signals. Averaging is performed over several image sequences acquired consecutively.

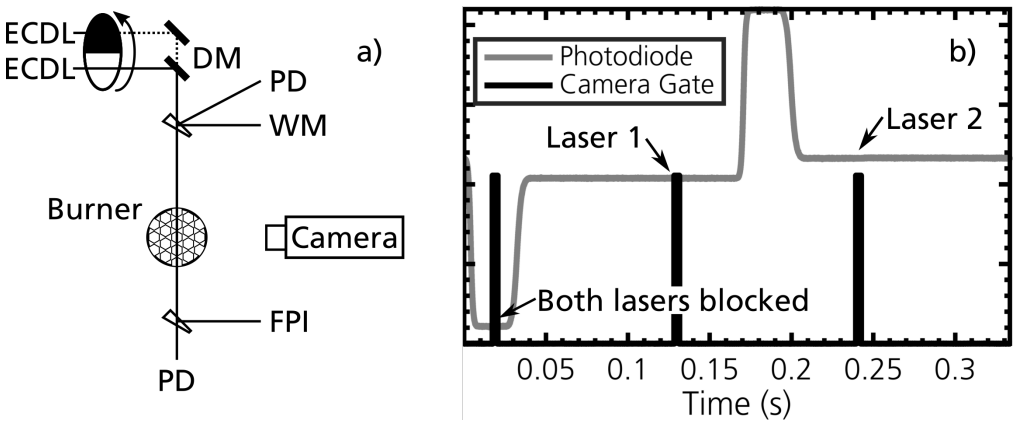

Figure 4.8: *a*) Schematic of the experimental setup used for fixed wavelength TLAF. ECDL - external-cavity diode laser, DM - dichroic mirror, WM - wavemeter, FPI - Fabry-Perot etalon. *b*) Reponse of a photodiode during a revolution of the chopper and the acquisitions of the camera.

After the chopper wheel the laser beams were overlapped with a dichroic mirror and sent first through a wedged glass plate and then into the interrogation region. A second wedged glass plate was aligned after the burner. The two reflections of the first glass plate was recorded on a reference photodiode calibrated to the laser power and a wavemeter. The two beams from the second glass plate was sent to a second photodiode for absorption measurement and a scanning Fabry-Perot etalon to verify that the lasers were running in single-mode. More details are presented in Paper III.

A line shape was recorded by changing the wavelength of the laser in discrete steps and recording the resulting fluorescence and the wavemeter reading. The line shape is, as discussed earlier, important for the accuracy of the technique. The best results were achieved when the experimental procedure explained above was used, i.e. recording the LIF and background every other image. The experimentally measured line shapes of indium and gallium are shown in Figure 4.9 as well as the best fitted line shape and peak positions of the individual hyperfine transitions using the atomic data presented in Chapter 5.1. The line shape is seen to be narrower for gallium than for indium due to the more closely spaced hyperfine lines, although, the broadening due to pressure and temperature diminishes this difference. The lasers were tuned to the peak of the line shapes, marked by red circles in the figure, when the temperature measurements were conducted.

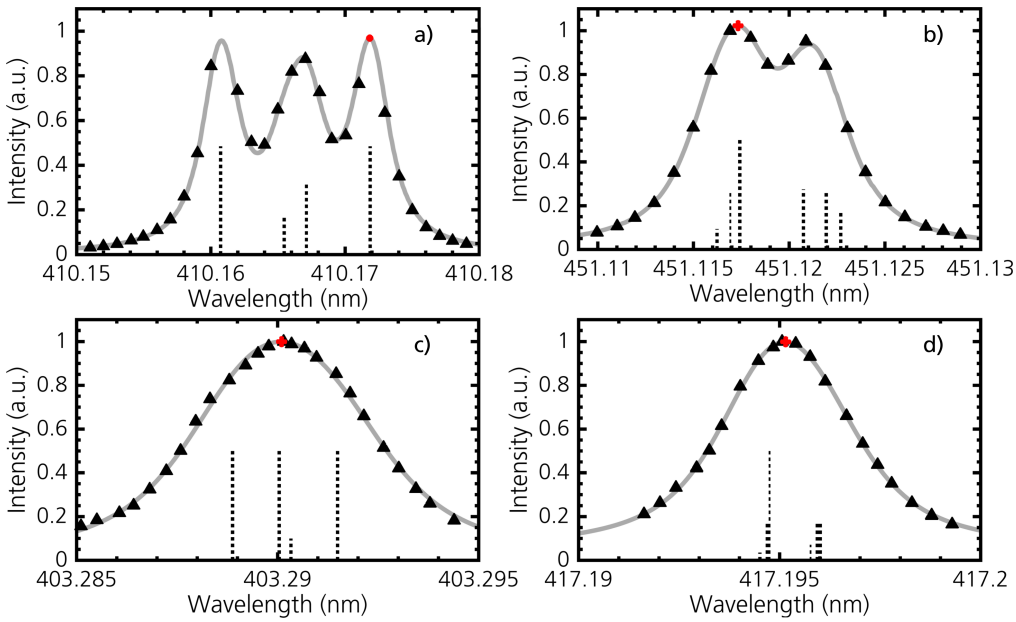

Figure 4.9: The line shapes of the two selected transitions of indium and gallium as reported in Paper III. Triangles show the experimental data, grey lines the best fit and red circles the peak of the absoprtion profile the lasers were tuned to during the temperature measurements. The individual hyperfine transitions are also shown as the dotted lines underneath each line shape. The relative intensities are scaled by half their real intensity for visibilty purposes. *a*) Indium $5P_{1/2} \rightarrow 6S_{1/2}$, *b*) Indium $5P_{3/2} \rightarrow 6S_{1/2}$, *c*) Gallium $4P_{1/2} \rightarrow 5S_{1/2}$ and *d*) Gallium $4P_{3/2} \rightarrow 5S_{1/2}$

A photograph of the laser-induced fluorescence of indium above the multi-jet burner running a stoichiometric methane/air-flame is shown in Figure 4.10a. The corresponding background-corrected laser-induced fluorescence of the $5P_{1/2} \rightarrow 6S_{1/2}$ transition of indium is seen in Figure 4.10b and the LIF profile, i.e. the averaged LIF signal across the whole height of the beam, is shown in Figure 4.10c for both transitions of indium. The indium concentration is observed to vary slightly across the burner most likely due to an inhomogeneous seeding arrangement. The temperature profile corresponding to the LIF signals is however flat, Figure 4.10d.

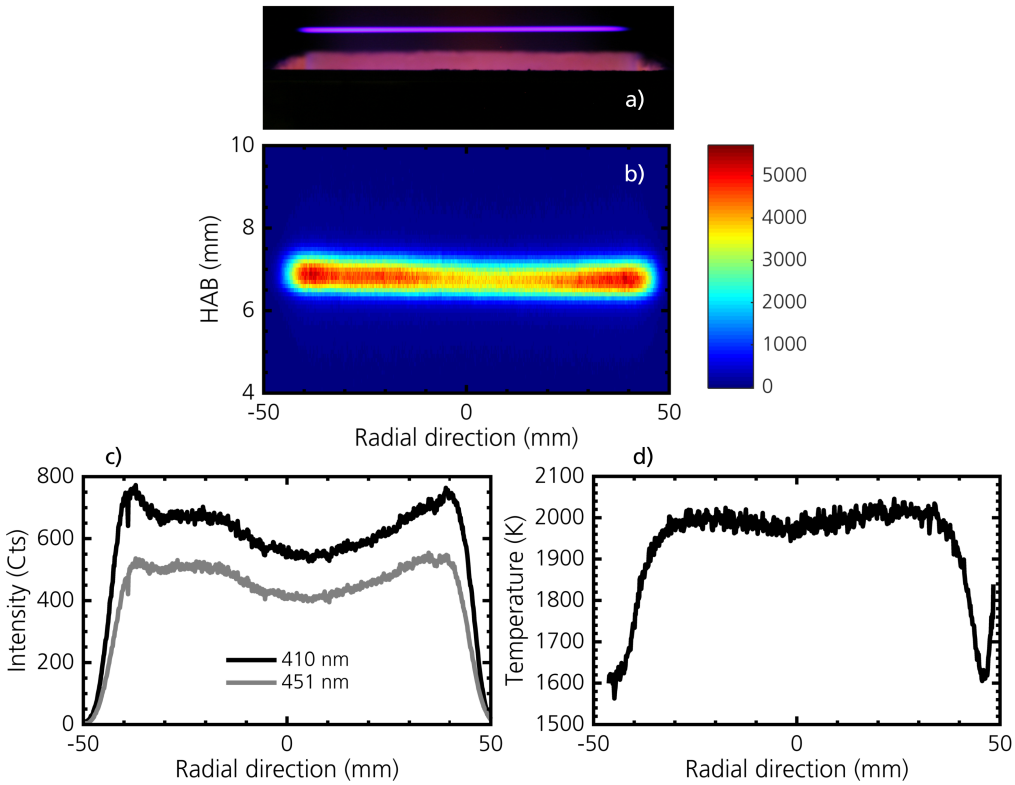

Figure 4.10: *a*) Photograph of the laser-induced fluorescence in a stoichimetric flame above the multi-jet burner. *b*) The recorded LIF of the 403 nm laser on the ICCD camera. *c*) The LIF profiles for the 410 nm and 451 nm lasers in the stoiciometric flame. *d*) The temperature profile derived from the LIF profiles presented in *c*.

In Figure 4.11 the average temperature in the flat part of the temperature profile is shown as a function of flame equivalence ratio for TLAF of indium and gallium as well as the measured CARS temperatures. The error bars show the standard deviation of three separate measurements taken at different days. The absolute temperature of the two atomic elements agree with each other within the experimental uncertainty. The TLAF temperature measurements were compared to rotational CARS measurements and also here the agreement is good, validating the fixed wavelength TLAF technique as an option for thermometric measurements in flames.

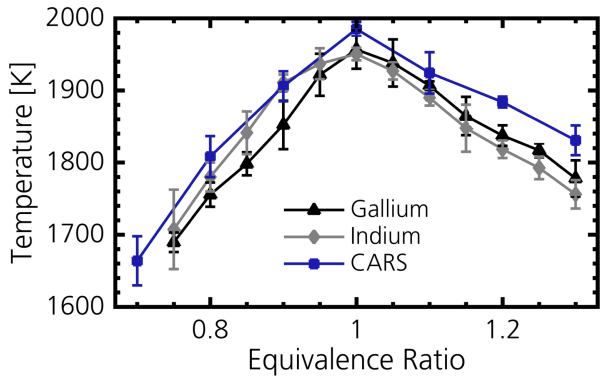

Figure 4.11: The average temperature of the flat region of the flame for TLAF of indium and gallium compared to rotational CARS. The error bars show the standard deviation of three individual measurements taken at different days.

4.3.1 LIDAR-based measurements

In most types of conventional laser-induced fluorescence imaging experiments the camera recording the LIF is located perpendicular to the direction of the laser sheet to achieve the optimal imaging conditions in terms of spatial resolution. The optical access required for this type of setup is not always available and in such cases special instrumentation e.g., endoscopes [89, 90] and fibers [4, 91] is needed. Another measurement technique that has great potential for measurements in environments with limited optical access is light-detection and ranging (LIDAR) measurements. In traditional LIDAR experiments a pulsed laser with the spectral characteristics necessary to probe a physical quantity is sent through the atmosphere [31]. The back-scattered light as the laser pulse interacts with matter is detected and temporally resolved on a fast photodetector. The temporal response can be converted to a length-based scale as the speed-of-light is well-known. If the laser is tuned to the transition of a molecule the concentration of this molecule can be measured over hundreds of metres [92–94].

The spatial resolution of LIDAR measurements is limited by the pulse length and detector bandwidth and in combustion experiments the spatial scales are much smaller than what is possible to resolve with traditional nanosecond-pulsed LIDAR. With the use of pico-second lasers it is possible to improve the spatial resolution to allow for measurements in enclosed combustion systems [95, 96], however, it requires the use of a very fast detector such as a streak camera. Kaldvee et al. [97] has demonstrated LIDAR-based single-ended thermometric measurements using Rayleigh scattering in a furnace. Temperatures up to 1200 K were measured and the spatial resolution was estimated to $\approx$ 6 cm. The expensive

equipment in the form of a picosecond-laser system and streak camera as well as the limited spatial resolution does, however, limit the adoption of pulsed LIDAR measurements for single-ended combustion experiments.

A novel LIDAR concept based on continuous-wave diode-lasers have recently been demonstrated by Mei et al. [98, 99]. In this LIDAR concept the imaging system is aligned according to the Scheimpflug principle to provide spatially resolved measurements. In the Scheimpflug setup the image, and lens axes are tilted to intersect in a single point with the plane of focus see Figure 4.12. Using this approach it is possible to simultaneously achieve a focus both close to, and far away from the detector[98]. In Scheimpflug LIDAR (sLIDAR) the spatial resolution is limited by the imaging optics and optical arrangement and not on the temporal pulse width of a laser, and the spatial resolution is therefore vastly improved. The spatial resolution follows a non-linear relationship that is dependent on several parameters, e.g., the collection optics and beam diameter. The spatial resolution deteriorates for objects further from the detector i.e. pixels recording signal further away from the detector images a larger part of space. This non-linear behaviour is not only a disadvantage, however, as the normal signal decrease of one over the distance squared ($1/R^2$) is counter-acted by the increasing imaging size per pixel [99].

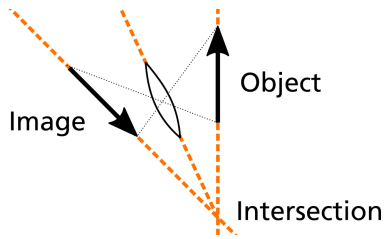

Figure 4.12: Schematic of the Scheimpflug principle. The three axes' of the image, lens and object plane intersect in a single point to achieve a tilted plane of focus relative to the detector.

The sLIDAR concept is ideal for single-ended spatially resolved temperature measurements with diode-laser based TLAF. For this purpose the sLIDAR concept was incorporated in the fixed wavelength TLAF setup described in Section 4.3. A schematic of the experimental setup of sLIDAR is shown in Figure 4.13. The two major differences to the measurements presented previously are that a set of lenses were used to shape the laser beam into a sheet with a height of approximately 5 mm and the intensified CCD camera was mounted in a Scheimpflug configuration. A modified Perkin-Elmer burner seeded with water-dissolved $InCl_3$ was located 2 metres from the camera. A stabilizer was mounted 23 mm above the burner. On the right of Figure 4.13 is the measured spatial scale along the direction of the laser beam as a function of pixel number on the camera chip showing a quadratic behaviour.

The beam profiles were characterized by measuring the elastic scattering of a very fine water mist flowed through the burner.

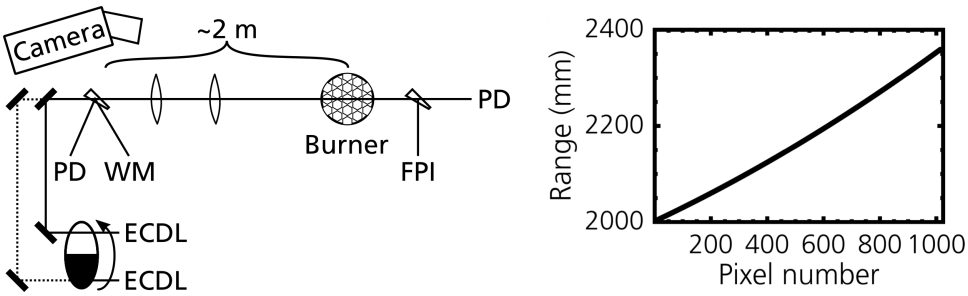

Figure 4.13: The Scheimpflug LIDAR TLAF setup. PD - photodiode, WM - wavemeter, FPI - Fabry-Perot Etalon and ECDL - external-cavity diode laser. The drawing is not scaled correctly. For real-world measurements the FPI could easily be placed with the other optical components close to the laser sources. The curve to the right shows the non-linear behviour of the range scale as a function of the pixel number on the camera chip.

Fixed wavelength temperature measurements using the resonant detection scheme were conducted by acquiring 200 image sequences as explained in Section 4.3, i.e. the two LIF signals and the background were each averaged over 200 images. The temperature distribution of a flame with equivalence ratio is shown in Figure 4.14 as well as the vertical and horizontal cross-sections corresponding to areas marked in the two-dimensional images. A flat temperature is observed both in the vertical and horizontal direction at this height above the burner. The accuracy is not affected by the use of the sLIDAR setup and is the same as reported in Paper III with an accuracy of $\approx$ 2.5 %.

These initial results shows that the Sheimpflug LIDAR concept could be used for diode-based TLAF measurements and provide accurate single-ended temperature measurements. The measurements can be conducted either with fast line scan detectors with kHz acquisition rates to provide fast one-dimensional temperature information or with ICCD-cameras for two-dimensional temperatures across relatively long distances in regards to combustion diagnostics.

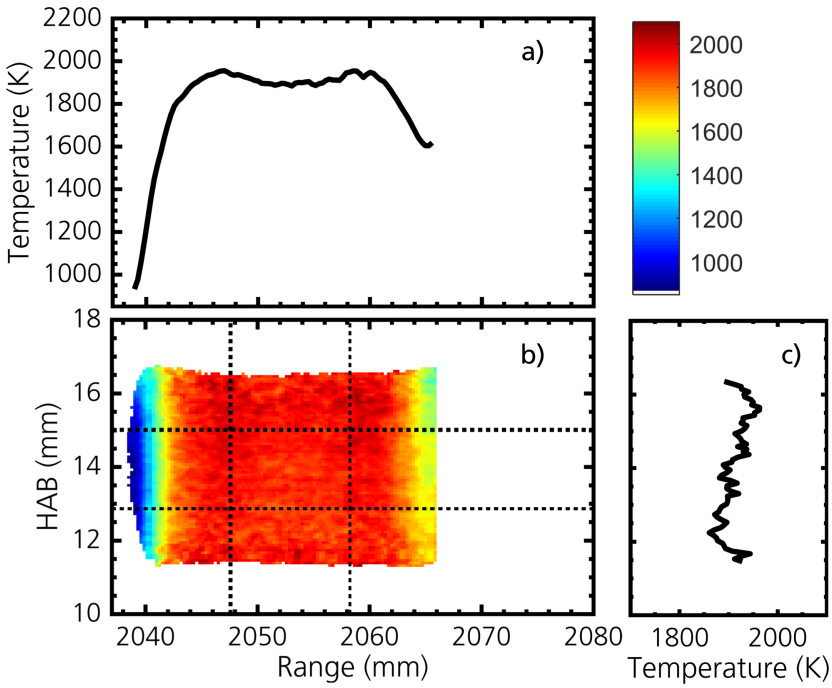

Figure 4.14: Temperature of a flame with equivalence ratio 1.2 measured with the sLIDAR setup. *a*) Horizontal temperature profile marked by the horizontal lines in *b*. *b*) Two-dimensional temperature distribution of the flame. *c*) The temperature profile as a function of height above burner (HAB) marked by the vertical lines in *b*.

4.4 Sooty and Particulate Laden Flames

The TLAF technique has the advantage of being able to measure temperatures in sooty and particulate laden flames [100, 101] as the detected wavelengths may be spectrally shifted from the excitation wavelengths, see Section 2.3.2. However, these types of TLAF measurements normally requires a second thermometric measurement to calibrate the optical setup due to e.g., differences in quantum efficiencies of the detectors at the two wavelengths. This limits the accuracy of the TLAF measurements to that of the calibration technique. In Paper IV diode-laser-based TLAF for sooty and particulate laden flames is reported in which the calibration is performed with the same setup thus making the thermometric measurements independent of another calibration technique.

For the measurements performed in Paper IV a single ICCD camera was mounted with a stereoscope producing two separate images on the CCD-chip. The two openings of the stereoscope were mounted with the bandpass filters for the two wavelengths of gallium

to spectrally filter the detected signal. The combustion of biomass pellets produces a sooty environment due to the diffusion flame formed from the combustion of the released volatile gases during heating of the pellet. A photograph of a burning wood pellet placed in the flue gas of a premixed methane-air flame of equivalence ratio 0.9 is shown in Figure 4.15. The laser beams were aligned 10 mm above the wood pellet and the laser-induced fluorescence is clearly seen in the photograph.

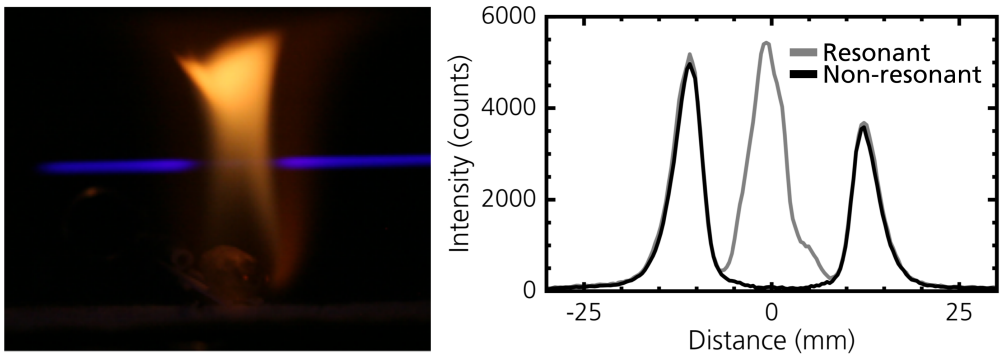

Figure 4.15: *Left* - Photograph of a burning pellet. The laser-induced fluorescence of gallium is observed as the blue line above the pellet. *Right* - The detect non-resonant and resonant LIF signal taken at approximately the same time as the photograph to the left.

The right graph in Figure 4.15 shows the LIF signal recorded on the ICCD-camera upon excitation from the 403 nm laser detected with the two filters. A strong LIF signal is observed in at the edges of the diffusion flame due to the increased local equivalence ratio. The concentration of the seeded species has previously been observed to have a strong dependence on the equivalence ratio of the flame [65, 100]. At lean flame conditions the concentration decreases rapidly due to oxidation with radicals more abundant at these leaner flame conditions. For the resonantly detected LIF a strong scattering signal is observed above the centre of the pellet. This elastic scattering signal is not present in the non-resonantly detected LIF. The advantage of this type of detection scheme for measurements in sooty environments is obvious as accurate temperature measurements would not be possible otherwise.

Chapter 5

Summary and Outlook

The work presented throughout this thesis covers the development and application of two-line atomic fluorescence for thermometric measurements in reactive flows. The focus of the research has been dedicated to diode-laser-based measurements. Diode lasers provide compact and robust experimental setups and offers a wavelength stability and control that allows for accurate investigations of the absorption profiles of the probed atomic species. Two variations of diode-laser-based TLAF have been demonstrated in the included papers, line shape resolved and fixed wavelength TLAF. The low laser power of diode lasers limits the temporal resolution to time averaged measurements. The main findings and results are itemised below and in the next section an outlook of future work is given.

- The development of the atomic seeding system described in Paper I improves the introduction of the atomic species for TLAF in comparison to traditional seeding arrangements involving water-soluble salts. The seeding system, based on the seeding of organometallic substances in gas phase, is versatile and applicable in a wide range of combustion environments and provides a stable flow of the seeded species.

- In Paper III indium and gallium was compared as temperature markers for TLAF. The two temperature markers were found to behave similarly at flame temperatures and no notable difference in accuracy was observed using the fixed wavelength technique. This paper demonstrates how the organometallic substance may easily be changed with the developed seeding system.

- Two-dimensional temperature measurements were acquired on an intensified high-speed camera in a low-pressure burner using the line shape resolved technique. This

type of measurement provides three independent temperature measurements simultaneously: two measurements from the fitting of each line shape (OLAF) and one measurement derived from the TLAF expression. These three measured temperatures were all observed to agree within the accuracy of each technique for all positions in the flame.

- In atmospheric flames a fixed wavelength TLAF technique was adopted where the lasers were tuned and kept fixed to the peak of the absorption profiles for each temperature measurement. In fixed wavelength TLAF the more commonly available ICCD camera can be used instead of a high-speed camera and the temporal resolution of these types of measurements is higher compared to line shape resolved TLAF. This TLAF technique displayed good agreement with rotational CARS measurements.

- The accuracy and precision of the developed thermometric techniques have been carefully investigated. A large error source comes from erroneous quantification of the laser power and this error is common for both presented techniques. Wavelength drifts and the line shape fitting parameters are other error sources that has to be accounted for. In conclusion the accuracies were found to be within 2-3 % at flame temperatures for the two techniques with precisions below 1 % for averaged measurements.

- Temporally resolved measurements are demonstrated in Paper IV. Here, the slow combustion processes of a biomass pellet placed in the hot product gas of a laminar flame was temporally and spatially resolved. The need for spatially resolved measurements are clearly displayed in these measurements. The decrease in temperature above the pellet as volatile gases are released are difficult to quantify with line-of-sight techniques.

5.1 Future Work

The renewed interest of TLAF over the past decade and the subsequent research has increased the knowledge of this thermometric technique considerably. The research has been both of a fundamental and applied nature, often with the two aspects being coupled. Fundamental research may include improvements to the precision and accuracy as well as better characterisation of the fundamental constants of the temperature marker. An example being the recent extension of TLAF to the non-linear and saturated excitation regime striving to increase the precision of the technique. With all these technical advancements TLAF

becomes a more mature diagnostic technique. Nevertheless, there are still improvements to be made and in the following section some suggestions of future work are presented.

TLAF measurements conducted in the saturation (sTLAF) regime has proven useful to increase the signal-to-noise ratio and thereby also the precision of the temperature measurements. However; the temperature expression of sTLAF becomes dependent on several atomic properties, e.g., the relaxation rate between the two lower levels. This relaxation rate is not well-known for flame conditions but could possibly be quantified by using short laser pulses from picosecond lasers in combination with an overlapped continuous-wave diode laser (ECDL). Procedurally the pulsed laser is tuned to one of the transitions of the atomic species and the diode lasers is tuned to the other transition. The intensity of the diode laser is temporally resolved during and after excitation from the pulsed laser on a fast detector. The detected signal would allow for the relaxation between the two lower levels to be measured. This information could be useful when deriving the temperature in sTLAF and show how this relaxation rate depends on the temperature and gas composition.

Increasing the measurable temperature range of TLAF is useful in many applications, e.g., in temperature measurements of the unburned gas region and pre-ignition in internal combustion engines. The expected temperatures at these locations and times are much lower than flame temperatures and TLAF has not been able to provide temperature information at these lower temperatures. TLAF has been restricted by the limited temperature range of the seeded species (indium) or the lack of ability to generate free atoms before the reaction zone. Combining a method for generation of free atoms at low temperatures and gallium could potentially allow temperatures as low as 400 K to be measured. Two possible solutions would be to either pre-heat the TMGa carrier gas to induce thermal decomposition of the organometallic substance or alternatively photo-dissociate the seeded molecules with a UV laser pulse.

In combustion environments where the pressure changes with time such as in internal combustion engines the shift and broadening induced by the pressure have to be considered. Doppler-free spectroscopy techniques can be used to quantify the pressure broadening in different flame conditions and pressures. Saturation spectroscopy or polarization spectroscopy with counter-propagating beams is examples of Doppler-free techniques. Even the low power diode lassers have been shown to reach saturating energies if tightly focussed allowing for saturation spectroscopy to be performed. The pressure-shift can be quantified by simultaneously recording the line shape in flame located in pressure cell and a fixed reference such as a hollow-cathode lamp with the atomic species at hand. The line shape of the hollow-cathode lamp will always be at the same position while the line shape from the absorption in the flame will vary with the pressure of the flame. The pressure shift as a function of gas composition can also be investigated similarly by varying the equivalence

ratio.

A single-mode injection-seeded OPO is described in Chapter 3 in an attempt to improve the accuracy of single-shot TLAF measurements. The beam profile and stability of the laser was found to be somewhat lacking thus limiting the applicability of the OPO in temperature measurements. Additional work is required to improve these parameters of the laser and especially the beam profile. An active feedback for the cavity length and possibly changing the crystal angle would allow for better control of the OPO wavelength. A ring cavity configuration may simplify the injection seeding procedure as the back reflections are removed.

Acknowledgement

The years I have spent at Combustion Physics have been a fantastic journey thanks to the amazing people I have had the privilege to get acquainted with. The PhD can sometimes be a sisyphean challenge and without support it is easy to succumb. My journey would not have been the same without my colleagues providing the excellent atmosphere and working environment, and for that I am grateful.

I would like to thank my supervisors Zhongshan and Marcus for challenging me with fascinating and demanding tasks. I also appreciate the loose reins I was given that allowed me to pursue areas of research that piqued my interest.

Thank you to all the people that I have had the pleasure to work with and especially to all the co-authors of the papers.

My office mate for the majority of my PhD journey, Bo Zhou, deserves a special thanks for always being ready to discuss and help me solve many of the problems that I encountered during my PhD.

Thank you Fahed for making our banishment to the lab floor so much more enjoyable. You are a great friend who is always there when I have needed it. To all the fantastic people that I've spent time with outside of work, Nils-Erik, Rickard, Jocke, Emil, Moah, Johan, and all the rest of you who know who you are deserves an acknowledgement. There are of course many more people that should be named, however, at the time of me writing this acknowledgement in the last hours before printing, you might have slipped my mind (or I ran out of time). I hope you don't hold it against me.

The last couple of years have been tumultuous and I am very thankful that I have you, Malin, by side to support me in this "hurricane". You mean the world to me. Slutligen, vill jag också tacka min familj och släkt för all uppmuntran jag har fått genom åren. Det är ni som har gjort det här möjligt.

Bibliography

[1] G. Nathan, P. Kalt, Z. Alwahabi, B. Dally, P. Medwell, and Q. Chan. Recent advances in the measurement of strongly radiating, turbulent reacting flows. *Progress in Energy and Combustion Science*, 38(1):41–61, 2012.

[2] A. Ehn, J. Zhu, X. Li, and J. Kiefer. Advanced Laser-Based Techniques for Gas-Phase Diagnostics in Combustion and Aerospace Engineering. *Applied Spectroscopy*, 71(3):341–366, 2017.

[3] A. C. Eckbreth. *Laser diagnostics for combustion temperature and species*, volume 3. CRC Press, 1996.

[4] K. Kohse-Höinghaus and J. B. Jeffries. *Applied combustion diagnostics*. Taylor & Francis, 2002.

[5] S. J. Blundell and K. M. Blundell. *Concepts in thermal physics*. OUP Oxford, 2009.

[6] P. Atkins. *The Laws of Thermodynamics: A Very Short Introduction*. OUP Oxford, 2010.

[7] G. Jönsson. *Fysik i vätskor och gaser*. Media-Tryck, 2016.

[8] S. R. Turns. *Thermodynamics: concepts and applications*. Cambridge University Press, 2006.

[9] C. T. J. Alkemade and R. Herrmann. *Fundamentals of analytical flame spectroscopy*. Wiley, New York :, 1979.

[10] R. B. Miles, W. R. Lempert, and J. N. Forkey. Laser rayleigh scattering. *Measurement Science and Technology*, 12(5):R33, 2001.

[11] J. Zetterberg, Z. Li, M. Afzelius, and M. Alden. Two-Dimensional Temperature Measurements in Flames Using Filtered Rayleigh Scattering at 254 nm. *Applied Spectroscopy*, 62(7):778–783, 2008.

[12] D. Hoffman, K.-U. Münch, and A. Leipertz. Two-dimensional temperature determination in sooting flames by filtered Rayleigh scattering. *Optics letters*, 21(7):525–527, 1996.

[13] A. Bohlin, M. Mann, B. D. Patterson, A. Dreizler, and C. J. Kliewer. Development of two-beam femtosecond/picosecond one-dimensional rotational coherent anti-Stokes Raman spectroscopy: Time-resolved probing of flame wall interactions. *Proceedings of the Combustion Institute*, 35(3):3723 – 3730, 2015.

[14] A. Bohlin and C. J. Kliewer. Communication: Two-dimensional gas-phase coherent anti-Stokes Raman spectroscopy (2D-CARS): Simultaneous planar imaging and multiplex spectroscopy in a single laser shot. *The Journal of Chemical Physics*, 138(22):221101, 2013.

[15] J. D. Miller, M. N. Slipchenko, T. R. Meyer, H. U. Stauffer, and J. R. Gord. Hybrid femtosecond/picosecond coherent anti-Stokes Raman scattering for high-speed gas-phase thermometry. *Optics letters*, 35(14):2430–2432, 2010.

[16] C. Abram, B. Fond, and F. Beyrau. Temperature measurement techniques for gas and liquid flows using thermographic phosphor tracer particles. *Progress in Energy and Combustion Science*, 64(Supplement C):93 – 156, 2018.

[17] W. G. Bessler, F. Hildenbrand, and C. Schulz. Two-line laser-induced fluorescence imaging of vibrational temperatures in a NO-seeded flame. *Appl. Opt.*, 40(6):748–756, Feb 2001.

[18] R. Giezendanner-Thoben, U. Meier, W. Meier, J. Heinze, and M. Aigner. Phase-locked two-line OH planar laser-induced fluorescence thermometry in a pulsating gas turbine model combustor at atmospheric pressure. *Appl. Opt.*, 44(31):6565–6577, Nov 2005.

[19] R. Devillers, G. Bruneaux, and C. Schulz. Development of a two-line OH-laser-induced fluorescence thermometry diagnostics strategy for gas-phase temperature measurements in engines. *Applied optics*, 47(31):5871–5885, 2008.

[20] U. E. Meier, D. Wolff-Gaßmann, and W. Stricker. LIF imaging and 2D temperature mapping in a model combustor at elevated pressure. *Aerospace Science and Technology*, 4(6):403 – 414, 2000.

[21] B. Williams, M. Edwards, R. Stone, J. Williams, and P. Ewart. High precision in-cylinder gas thermometry using Laser Induced Gratings: Quantitative measurement of evaporative cooling with gasoline/alcohol blends in a GDI optical engine. *Combustion and Flame*, 161(1):270 – 279, 2014.

[22] E. Condon and G. Shortley. *The Theory of Atomic Spectra*. Cambridge Univ.Pr.209. Cambridge University Press, 1951.

[23] A. Manteghi, Y. Shoshin, N. J. Dam, and L. P. H. Goey. Two-line atomic fluorescence thermometry in the saturation regime. *Applied Physics B*, 118(2):281–293, 2014.

[24] G. Zizak, J. Bradshaw, and J. Winefordner. Rate equation solution for the temporal behavior of a three-level system. *Applied optics*, 19(21):3631–3639, 1980.

[25] R. C. Hilborn. Einstein coefficients, cross sections, f values, dipole moments, and all that. *American Journal of Physics*, 50(11):982–986, 1982.

[26] R. S. M. Chrystie. *Development of novel laser diagnostic techniques for the quantitative study of premixed flames*. PhD thesis, University of Cambridge, 2009.

[27] J. E. Dec and J. O. Keller. High speed thermometry using two-line atomic fluorescence. *Symposium (International) on Combustion*, 21(1):1737–1745, 1988.

[28] J. Hult, I. S. Burns, and C. F. Kaminski. Measurements of the indium hyperfine structurein an atmospheric-pressure flameby use of diode-laser-induced fluorescence. *Opt. Lett.*, 29(8):827–829, 2004.

[29] P. R. Medwell, Q. N. Chan, P. A. M. Kalt, Z. T. Alwahabi, B. B. Dally, and G. J. Nathan. Development of temperature imaging using two-line atomic fluorescence. *Appl. Opt.*, 48(6):1237–1248, 2009.

[30] P. R. Medwell, Q. N. Chan, P. A. M. Kalt, Z. T. Alwahabi, B. B. Dally, and G. J. Nathan. Instantaneous Temperature Imaging of Diffusion Flames Using Two-Line Atomic Fluorescence. *Applied Spectroscopy*, 64(2):173–176, 2010.

[31] S. Svanberg. *Atomic and molecular spectroscopy: basic aspects and practical applications*, volume 6. Springer Science & Business Media, 2012.

[32] W. Demtröder. *Laser spectroscopy: basic concepts and instrumentation*. Springer Science & Business Media, 2013.

[33] O. Axner, J. Gustafsson, N. Omenetto, and J. D. Winefordner. Line strengths, A-factors, and absorption cross sections for lines and hyperfine structure components in atomic spec-

trometry : A user's approach. *Spectrochimica Acta Part B - Atomic Spectroscopy*, 59(1):1–39, 2004.

[34] I. S. Burns, J. Hult, G. Hartung, and C. F. Kaminski. A thermometry technique based on atomic lineshapes using diode laser LIF in flames. *Proceedings of the Combustion Institute*, 31(1):775–782, 2007.

[35] I. I. Sobel'Man, L. A. Vainshtein, and E. A. Yukov. *Excitation of atoms and broadening of spectral lines*, volume 15. Springer Science & Business Media, 2012.

[36] A. P. Nefedov, V. A. Sinel'shchikov, and A. D. Usachev. Collisional Broadening of the Na-D Lines by Molecular Gases. *Physica Scripta*, 59(6):432, 1999.

[37] T. Leffler. *Development and Application of Optical Diagnostics of Alkali Vapours for Solid Fuel Combustion*. PhD thesis, Lund University, 2016.

[38] T. T. Kajava, H. M. Lauranto, and R. R. E. Salomaa. Mode structure fluctuations in a pulsed dye laser. *Appl. Opt.*, 31(33):6987–6992, Nov 1992.

[39] L. A. Westling, M. G. Raymer, and J. J. Snyder. Single-shot spectral measurements and mode correlations in a multimode pulsed dye laser. *J. Opt. Soc. Am. B*, 1(2):150–154, Apr 1984.

[40] I. S. Burns, X. Mercier, M. Wartel, R. S. M. Chrystie, J. Hult, and C. F. Kaminski. A method for performing high accuracy temperature measurements in low-pressure sooting flames using two-line atomic fluorescence. *Proceedings of the Combustion Institute*, 33(1):799–806, 2011.

[41] J. Eberz, G. Huber, T. Kuhl, and G. Ulm. Pressure broadening and pressure shift of the 410 nm indium line perturbed by foreign gases. *Journal of Physics B: Atomic and Molecular Physics*, 17(15):3075, 1984.

[42] K. MacAdam, A. Steinbach, and C. Wieman. A narrow-band tunable diode laser system with grating feedback, and a saturated absorption spectrometer for Cs and Rb. *American Journal of Physics*, 60(12):1098–1111, 1992.

[43] L. Ricci, M. Weidemüller, T. Esslinger, A. Hemmerich, C. Zimmermann, V. Vuletic, W. König, and T. W. Hänsch. A compact grating-stabilized diode laser system for atomic physics. *Optics Communications*, 117(5):541–549, 1995.

[44] J. Hult, I. S. Burns, and C. F. Kaminski. Two-line atomic fluorescence flame thermometry using diode lasers. *Proceedings of the Combustion Institute*, 30(1):1535–1543, 2005.

[45] T. Hansch and B. Couillaud. Laser frequency stabilization by polarization spectroscopy of a reflecting reference cavity. *Optics Communications*, 35(3):441 – 444, 1980.

[46] R. W. P. Drever, J. L. Hall, F. V. Kowalski, J. Hough, G. M. Ford, A. J. Munley, and H. Ward. Laser phase and frequency stabilization using an optical resonator. *Applied Physics B*, 31(2):97–105, Jun 1983.

[47] T. W. Hänsch, I. S. Shahin, and A. L. Schawlow. High-Resolution Saturation Spectroscopy of the Sodium *D* Lines with a Pulsed Tunable Dye Laser. *Phys. Rev. Lett.*, 27:707–710, Sep 1971.

[48] V. V. Yashchuk, D. Budker, and J. R. Davis. Laser frequency stabilization using linear magneto-optics. *Review of Scientific Instruments*, 71(2):341–346, 2000.

[49] D. Kleinman. Theory of optical parametric noise. *Physical Review*, 174(3):1027, 1968.

[50] A. Fix and R. Wallenstein. Spectral properties of pulsed nanosecond optical parametric oscillators: experimental investigation and numerical analysis. *J. Opt. Soc. Am. B*, 13(11):2484–2497, Nov 1996.

[51] J. E. Bjorkholm and H. G. Danielmeyer. Frequency Control of a Pulsed Optical Parametric Oscillator by Radiation Injection. *Applied Physics Letters*, 15(6):171–173, 1969.

[52] A. H. Bhuiyan, D. R. Richardson, S. V. Naik, and R. P. Lucht. Development of an optical parametric generator with pulsed dye amplification for high-resolution laser spectroscopy. *Applied Physics B*, 94(4):559–567, 2009.

[53] J. A. J. Fitzpatrick, O. V. Chekhlov, J. M. F. Elks, C. M. Western, and S. H. Ashworth. An injection seeded narrow bandwidth pulsed optical parametric oscillator and its application to the investigation of hyperfine structure in the PF radical. *Journal of Chemical Physics*, 115:6920–6930, 2001.

[54] W. D. Kulatilaka, T. N. Anderson, T. L. Bougher, and R. P. Lucht. Development of injection-seeded, pulsed optical parametric generator/oscillator systems for high-resolution spectroscopy. *Applied Physics B: Lasers and Optics*, 80:669–680, 2005.

[55] M. J. T. Milton, T. D. Gardiner, G. Chourdakis, and P. T. Woods. Injection seeding of an infrared optical parametric oscillator with a tunable diode laser. *Opt. Lett.*, 19(4):281–283, 1994.

[56] M. Rahm, U. Bäder, G. Anstett, J. P. Meyn, R. Wallenstein, and A. Borsutzky. Pulse-to-pulse wavelength tuning of an injection seeded nanosecond optical parametric generator with 10Â kHz repetition rate. *Applied Physics B: Lasers and Optics*, 75:47–51, 2002.

[57] T. D. Raymond, M. S. Bowers, W. J. Alford, and A. V. Smith. Frequency shifts in injection-seeded optical parametric oscillators with phase mismatch. *Opt. Lett.*, 19(19):1520–1522, Oct 1994.

[58] T. Plessing, C. Kortschik, N. Peters, M. Mansour, and R. Cheng. Measurements of the turbulent burning velocity and the structure of premixed flames on a low-swirl burner. *Proceedings of the Combustion Institute*, 28(1):359–366, 2000.

[59] D. Yegian and R. Cheng. Development of a lean premixed low-swirl burner for low NOx practical applications. *Combustion science and technology*, 139(1):207–227, 1998.

[60] K. Bosschaart and L. De Goey. Detailed analysis of the heat flux method for measuring burning velocities. *Combustion and flame*, 132(1):170–180, 2003.

[61] N. Omenetto, P. Benetti, and G. Rossi. Flame temperature measurements by means of atomic fluorescence spectrometry. *Spectrochimica Acta Part B: Atomic Spectroscopy*, 27(10):453–461, 1972.

[62] H. Haraguchi, B. Smith, S. Weeks, D. J. Johnson, and J. D. Winefordner. Measurement of Small Volume Flame Temperatures by the Two-line Atomic Fluorescence Method. *Appl. Spectrosc.*, 31(2):156–163, 1977.

[63] R. G. Joklik and J. W. Daily. Two-line atomic fluorescence temperature measurement in flames: an experimental study. *Applied Optics*, 21(22):4158–4162, 1982.

[64] C. Kaminski, J. Engström, and M. Aldén. Quasi-instantaneous two-dimensional temperature measurements in a spark ignition engine using 2-line atomic fluorescence. In *Symposium (International) on Combustion*, volume 27, pages 85–93. Elsevier, 1998.

[65] Q. N. Chan, P. R. Medwell, P. A. M. Kalt, Z. T. Alwahabi, B. B. Dally, and G. J. Nathan. Solvent effects on two-line atomic fluorescence of indium. *Applied Optics*, 49(8):1257–1266, 2010.

[66] J. H. Gibson, W. E. L. Grossman, and W. D. Cooke. Excitation Processes in Flame Spectrometry. *Analytical Chemistry*, 35(3):266–277, 1963.

[67] J. D. Winefordner and H. W. Latz. Quantitative Study of Factors Influencing Sample Flow Rate in Flame Photometry. *Analytical Chemistry*, 33(12):1727–1732, 1961.

[68] I. Burns, N. Lamoureux, C. Kaminski, J. Hult, and P. Desgroux. Diode laser atomic fluorescence temperature measurements in low-pressure flames. *Applied Physics B*, 93:907–914, 2008.

[69] P. R. Medwell, Q. N. Chan, B. B. Dally, Z. T. Alwahabi, S. Mahmoud, G. F. Metha, and G. J. Nathan. Flow seeding with elemental metal species via an optical method. *Applied Physics B*, 107(3):665–668, Jun 2012.

[70] D. H. Gu, Z. W. Sun, P. R. Medwell, Z. T. Alwahabi, B. B. Dally, and G. J. Nathan. Mechanism for laser-induced fluorescence signal generation in a nanoparticle-seeded flow for planar flame thermometry. *Applied Physics B-Lasers and Optics*, 118(2):209–218, 2015.

[71] K. Tian, D. Snelling, and G. Smallwood. Application of arc-lamp based TLAF technique to temperature measurement in a laminar CH4/air diffusion flame. *Combustion Institute Canadian Section*, pages 1–5, 2005.

[72] D. V. Shenai-Khatkhate, R. L. DiCarlo, and R. A. Ware. Accurate vapor pressure equation for trimethylindium in OMVPE. *Journal of Crystal Growth*, 310(7):2395–2398, 2008.

[73] M. Fulem, K. Ruzicka, V. Ruzicka, T. Simecek, E. Hulicius, and J. Pangrac. Vapour pressure measurement of metal organic precursors used for {MOVPE}. *The Journal of Chemical Thermodynamics*, 38(3):312 – 322, 2006.

[74] A. Kramida, Y. Ralchenko, Reader, J., and NIST ASD Team. NIST Atomic Spectra Database, version (5.5.1) https://physics.nist.gov/asd, Retreived 2017-12-08.

[75] J. Nygren, J. Engström, J. Walewski, C. F. Kaminski, and M. Aldén. Applications and evaluation of two-line atomic LIF thermometry in sooting combustion environments. *Measurement Science and Technology*, 12(8):1294, 2001.

[76] F. Battin-Leclerc. Detailed chemical kinetic models for the low-temperature combustion of hydrocarbons with application to gasoline and diesel fuel surrogates. *Progress in Energy and Combustion Science*, 34(4):440 – 498, 2008.

[77] O. Welz, J. Zador, J. D. Savee, M. Y. Ng, G. Meloni, R. X. Fernandes, L. Sheps, B. A. Simmons, T. S. Lee, D. L. Osborn, and C. A. Taatjes. Low-temperature combustion chemistry of biofuels: pathways in the initial low-temperature (550 K-750 K) oxidation chemistry of isopentanol. *Phys. Chem. Chem. Phys.*, 14:3112–3127, 2012.

[78] Y. Ju, J. K. Lefkowitz, C. B. Reuter, S. H. Won, X. Yang, S. Yang, W. Sun, Z. Jiang, and Q. Chen. Plasma Assisted Low Temperature Combustion. *Plasma Chemistry and Plasma Processing*, 36(1):85–105, Jan 2016.

[79] A. Mcilroy, T. D. Hain, H. A. Michelsen, and T. A. Cool. A laser and molecular beam mass spectrometer study of low-pressure dimethyl ether flames. *Proceedings of the Combustion Institute*, 28(2):1647–1653, 2000.

[80] A. Frassoldati, T. Faravelli, E. Ranzi, K. Kohse-Höinghaus, and P. R. Westmoreland. Kinetic modeling study of ethanol and dimethyl ether addition to premixed low-pressure propene–oxygen–argon flames. *Combustion and Flame*, 158(7):1264–1276, 2011.

[81] Slavinskaya, N. A., Wiegand, M., Starcke, J. H., Riedel, U., Haidn, O. J., and Suslov, D. Kinetic mechanism for low-pressure oxygen/methane ignition and combustion. *EUCASS Proceedings Series: Advances in AeroSpace Sciences*, 4:707–732, 2013.

[82] P. Ifeacho, T. Huelser, H. Wiggers, C. Schulz, and P. Roth. Synthesis of SnO_{2-x} nanoparticles tuned between $0 \leq x \leq 1$ in a premixed low pressure H_2/O_2/Ar flame. *Proceedings of the Combustion Institute*, 31(2):1805–1812, 2007.

[83] M. T. Swihart. Vapor-phase synthesis of nanoparticles. *Current Opinion in Colloid & Interface Science*, 8(1):127–133, 2003.

[84] G. Skandan, Y. Chen, N. Glumac, and B. Kear. Synthesis of oxide nanoparticles in low pressure flames. *Nanostructured materials*, 11(2):149–158, 1999.

[85] E. Kristensson, A. Ehn, J. Bood, and M. Aldén. Advancements in Rayleigh scattering thermometry by means of structured illumination. *Proceedings of the Combustion Institute*, 35(3):3689–3696, 2015.

[86] A. Lawitzki, I. Plath, W. Stricker, J. Bittner, U. Meier, and K. Kohse-Höinghaus. Laser-induced fluorescence determination of flame temperatures in comparison with CARS measurements. *Applied Physics B*, 50(6):513–518, 1990.

[87] A. T. Hartlieb, B. Atakan, and K. Kohse-Höinghaus. Temperature measurement in fuel-rich non-sooting low-pressure hydrocarbon flames. *Applied Physics B*, 70(3):435–445, 2000.

[88] M. Tamura, J. Luque, J. Harrington, P. Berg, G. Smith, J. Jeffries, and D. Crosley. Laser-induced fluorescence of seeded nitric oxide as a flame thermometer. *Applied Physics B*, 66(4):503–510, Apr 1998.

[89] M. Wensing, M. Günther, A. Zboralski, and S. Liebsch. Endoscopic LIF in Combustion System Development. *MTZ worldwide*, 75(6):28–33, Jun 2014.

[90] S. Shawal, M. Goschutz, M. Schild, S. Kaiser, M. Neurohr, J. Pfeil, and T. Koch. High-Speed Imaging of Early Flame Growth in Spark-Ignited Engines Using Different Imaging Systems via Endoscopic and Full Optical Access. *SAE Int. J. Engines*, 9:704–718, 04 2016.

[91] P. S. Hsu, N. Jiang, A. K. Patnaik, V. Katta, S. Roy, and J. Gord. All-Fiber-Coupled OH Planar-Laser-Induced-Fluorescence-(OH-PLIF-)Based Two-Dimensional Thermometry. *Applied Spectroscopy*, 0(0):0003702817744519, 0.

[92] E. Browell, S. Ismail, and W. Grant. Differential absorption lidar (DIAL) measurements from air and space. *Applied Physics B: Lasers and Optics*, 67(4):399–410, 1998.

[93] P. Weibring, H. Edner, S. Svanberg, G. Cecchi, L. Pantani, R. Ferrara, and T. Caltabiano. Monitoring of volcanic sulphur dioxide emissions using differential absorption lidar (DIAL), differential optical absorption spectroscopy (DOAS), and correlation spectroscopy (COSPEC). *Applied Physics B: Lasers and Optics*, 67(4):419–426, 1998.

[94] A. M. South, I. M. Povey, and R. L. Jones. Broadband lidar measurements of tropospheric water vapor profiles. *Journal of Geophysical Research: Atmospheres*, 103(D23):31191–31202, 1998.

[95] B. Kaldvee, A. Ehn, J. Bood, and M. Aldén. Development of a picosecond lidar system for large-scale combustion diagnostics. *Appl. Opt.*, 48(4):B65–B72, Feb 2009.

[96] B. Kaldvee, C. Brackmann, M. Aldén, and J. Bood. LII–lidar: range-resolved backward picosecond laser-induced incandescence. *Applied Physics B*, 115(1):111–121, Apr 2014.

[97] B. Kaldvee, J. Bood, and M. Aldén. Picosecond-lidar thermometry in a measurement volume surrounded by highly scattering media. *Measurement Science and Technology*, 22(12):125302, 2011.

[98] L. Mei and M. Brydegaard. Continuous-wave differential absorption lidar. *Laser & Photonics Reviews*, 9(6):629–636, 2015.

[99] L. Mei and M. Brydegaard. Atmospheric aerosol monitoring by an elastic Scheimpflug lidar system. *Optics express*, 23(24):A1613–A1628, 2015.

[100] J. Engström, J. Nygren, M. Aldén, and C. F. Kaminski. Two-line atomic fluorescence as a temperature probe for highly sooting flames. *Opt. Lett.*, 25(19):1469–1471, 2000.

[101] Q. N. Chan, P. R. Medwell, P. A. M. Kalt, Z. T. Alwahabi, B. B. Dally, and G. J. Nathan. Simultaneous imaging of temperature and soot volume fraction. *Proceedings of the Combustion Institute*, 33(1):791–798, 2011.

[102] G. V. Deverall, K. W. Meissner, and G. J. Zissis. Hyperfine Structures of the Resonance Lines of Indium (In^{115}). *Phys. Rev.*, 91:297–299, 1953.

[103] O. M. Maragò, B. Fazio, P. G. Gucciardi, and E. Arimondo. Atomic gallium laser spectroscopy with violet/blue diode lasers. *Applied Physics B*, 77(8):809–815, 2003.

Summary of Papers

Paper I **Vapor phase tri-methyl-indium seeding system suitable for high temperature spectroscopy and thermometry.**

The development and application of a versatile system for seeding organometallics to a combustion environment is presented. The response of the seeding system was characterized when seeding trimethylindium to a laminar jet flame and was found to provide a stable concentration of indium to the flame. The distribution of indium atoms in the flame was investigated by laser-induced fluorescence and the concentration of indium atoms was measured as a function of expected TMI seeding concentration. The emission of indium radicals was spectrally characterized and the detected InOH radical was simulated using the PGopher software.

R. Whiddon designed and built the seeding system and performed most of the measurements with B. Zhou. I performed all the laser-based experiments and evaluated the data. I wrote the section of the manuscript that concerned the measurements that I had performed.

Paper II **Temperature imaging in low-pressure flames using diode laser two-line atomic fluorescence employing a novel indium seeding technique.**

Two-dimensional temperature measurements in a low-pressure flat flame is presented in this paper. The use of a high-speed camera allowed spatially resolved line shape resolved TLAF measurements to be performed. A TLAF evaluation routine based on least-squares fitting of the recorded line shapes was developed.

I planned most of the experiment and performed them with the help of A.L. Sahlberg and I. Burns. I developed the evaluation routine that required fitting of experimentally recorded line shapes. The data and error sources was evaluated by me and I wrote the manuscript with some input from I. Burns and Z.S. Li.

Paper III **Diode laser-based thermometry using two-line atomic fluorescence of indium and gallium.**

This two-part paper covers both the development and evaluation of the fixed wavelength TLAF technique as well as its application to investigate indium and gallium as temperature markers for TLAF at flame temperatures. The TLAF measurements were compared to CARS measurements and were found to agree well. No differences in regards to accuracy between indium and gallium were observed for these measurements.

I planned the experimental procedure and developed the evaluation routine. The experiment were mostly performed by me with some help from W. Weng. A. Hosseinnia was responsible for the CARS experiments and CARS section in the paper. I evaluated the TLAF data and wrote most of the manuscript.

Paper IV **Temperature measurements above a burning wood pellet using diode-laser based two-line atomic fluorescence..**

Fixed wavelength TLAF was extended to a non-resonant detection scheme to allow for temperature measurements in particle-laden and sooty flames. The technique was demonstrated above burning wood pellets in the multi-jet burner showing the need for spatially resolved measurements in these combustion processes.

I planned the experimental setup and measurement procedure on my own and conducted the measurements together with W. Weng. I evaluated the data and wrote the manuscript with some input from the other authors.

Paper V **A novel multi-jet burner for laminar flat flames of wide range of temperatures and oxygen concentrations: Valuable for quantitative optical diagnostics in biomass gasification/combustion.**

A multi-jet burner was developed to provide a wide range of combustion conditions such as temperatures ranging from 1000 K to 2000 K and seeding of gases and liquid solutions. The design of the burner is presented in this paper together with possible applications of the burner.

The main responsible for this paper was W. Weng who designed the burner. Together with W. Weng, I performed the experiments with trimethylindium for temperature measurements and provided input for the manuscript.

Appendix A

The atomic parameters regarding the hyperfine transitions used for simulation of the line shapes of indium and gallium.

Indium

Nuclear Angular Momentum I = 9/2
Electron Angular Momentum J = 3/2

Table A1: Atomic data for indium. F′ denotes the lower level and F″ upper level. Frequency spacing from [102] and relative intensities calculated with the Clebsch-Gordan coefficients.

Transition	Hyperfine transition (F' → F")	Frequency Spacing (GHz)	Relative Intensity
$5P_{1/2} \rightarrow 6S_{1/2}$	5 → 4	0	1
	5 → 5	8.436	0.6667
	4 → 4	11.413	0.3636
	4 → 5	19.849	1
$5P_{3/2} \rightarrow 6S_{1/2}$	5 → 4	0	0.3385
	4 → 4	1.084	0.5077
	3 → 4	1.753	0.5385
	6 → 5	6.650	1
	5 → 5	8.403	0.5077
	4 → 5	9.520	0.1846

Gallium

Nuclear Angular Momentum I = 3/2
Electron Angular Momentum J = 3/2

Table A2: Atomic data for gallium. F′ denotes the lower level and F″ upper level. Frequency spacing from [103] and relative intensities calculated with the Clebsch-Gordan coefficients.

Transition	Hyperfine transition (F' → F")	Frequency Spacing (GHz)	Relative Intensity
$4P_{1/2} \rightarrow 5S_{1/2}$	2 → 1	0	1
	2 → 2	2.1377	1
	1 → 1	2.6780	0.2
	1 → 2	4.8157	1
$4P_{3/2} \rightarrow 5S_{1/2}$	2 → 1	0	0.3571
	1 → 1	0.3191	0.3571
	0 → 1	0.4473	0.1429
	3 → 2	2.1377	1
	2 → 2	2.4568	0.3571
	1 → 2	2.5850	0.0714